INVESTIGATION ON MICROSTRUCTURE AND MECHANICAL PROPERTIES OF POROUS STRUCTURES PROCESSED BY LASER POWDER BED FUSION

by

SAMARTH RAMACHANDRA

Presented to the Faculty of the Graduate School of

The University of Texas at Arlington

in partial fulfillment of the requirements

for the degree of

MASTER OF SCIENCE IN MECHANICAL ENGINEERING

THE UNIVERSITY OF TEXAS AT ARLINGTON

May 2021

Acknowledgment

First and Foremost, I would like to express my sincere and utmost gratitude to Dr. Narges Shayesteh for all the invaluable guidance throughout the project and trusting me with this study and the equipment involved in this work. The unwavering vision, in-depth knowledge, patience, and dynamism that she has displayed at each point of the thesis work has immensely kept me motivated. Also, I greatly respect and appreciate her efforts in creating a sense of ease during the times of pandemic lockdown. I am also grateful to Dr. Amirhesam Amerinatanzi for his support and granting me the access to the necessary laboratories and resources without which none of this would have been possible.

I would also like to extend my gratitude to my friend Mr. Bharath Bhushan Ravichander for his constant support amidst his taxing schedule, with various aspects ranging from fabrication of the parts to conducting analyses along with compilation of my thesis document. I am also glad to have worked alongside Mr. Manjunath Hanumantha for he has provided genuine comments and suggestions on my work at various times.

Also, I deeply appreciate and thank the committee members Dr. Emma Yiran Yang and Dr. Md Rassel Raihan for taking time from their busy schedules to help me invariably propel my research work to fruition with their valuable inputs and feedback. This work would have largely remained incomplete without their presence.

I am always indebted to the perennial support and encouragement along with mounds of sacrifices that my parents have always displayed. Finally, I would also like to thank my friends and family for their unwavering support.

Abstract

INVESTIGATION ON MICROSTRUCTURE AND MECHANICAL PROPERTIES OF POROUS STRUCTURES PROCESSED BY LASER POWDER BED FUSION

Samarth Ramachandra, M.S

The University of Texas at Arlington, 2021

Supervising Professor: Dr. Narges Shayesteh

Inconel 718 (i.e., IN718) is a prominent nickel-based, precipitation-hardening superalloy which exhibits exceptionally stable mechanical and corrosion resistant properties, even at temperature range of 650ºC to 700ºC, making it suitable for a wide range of applications such as aerospace, nuclear reactors, tooling, turbines, oil and gas applications. The high toughness and work hardening offered by this superalloy, however, greatly limits the choice of machinability. The presence of low levels of aluminum permits good weldability which further allows the use of laser-based additive manufacturing (AM) to efficiently fabricate IN718 parts without the limitations associated with conventional manufacturing methods. Thanks to AM techniques, it is possible to even fabricate parts with complex geometries, such as porous structures, thin walls, and curved surfaces. Implementation of engineered porosity in an IN718 part successively promotes further advantages such as reduced weight and material use, making them great candidates for lightweight applications such as aerospace, space, automobile, biomedicine, and defense industries.

The porous structures commonly used in AM have been greatly inspired by the biological patterns and other naturally occurring structures such as honeycomb, molecular lattice cubic structures (e.g., FCC, FCC-Z, BCC, BCC-Z) and triply periodic minimal surface structures (e.g., Schwarz, gyroid and diamond). Different porous structures tend to have varied effects on the mechanical properties of the part based on the material used. While low density parts with enhanced local surface area can be fabricated for most of the materials along with other desired qualities, the key to obtain a part with optimized mechanical attributes is the right combination of the porous type and porosity level corresponding to the material involved.

In this study, IN718 structures with different porosity type and level are studies in terms of their microstructure and mechanical properties. To this aim, compression and hardness tests are conducted on all the test samples to obtain the mechanical properties. Also, compositional analysis using X-ray powder diffraction (XRD), and microstructural analysis using scanning electron microscope (SEM), are carried out on the specimens to study the defects and causes of failure. Through these tests and analyses, the process-structure-property relationship for porous IN718 are also identified, which could be used as a basis for optimization of process parameters to achieve better mechanical properties and part quality.

Table of contents

List of Tables

List of Figures

Chapter 1. Introduction

1.1. Motivation

Additive Manufacturing enables the possibility of flexible/organic part designs and implementation of porous structures on the fabrication of parts. As a result, with appropriate controlled parameters desired mechanical properties can be achieved [1]. However, the possibility of microstructural defects such as unmelted powder, cracks, impurities, etc. could still present challenges against the desired characteristics in a part. These defects may reduce the qualities such as tensile and compressive strengths, stiffness, capacity to absorb energy, and lead to premature failures. By observing such defects through the help of microstructure analysis, necessary post processing measures can be implemented to rectify or minimize such effects.

1.2. Objectives

The primary focus of this work is to study the effects of porosity type on microstructural and mechanical properties of IN718 parts fabricated on an EOS M290 Metal 3D printer. Additionally, conducting hardness and compression tests with further investigations using SEM, it is crucial to outline the microstructure – mechanical property relationship considering the effects of porosity, defects and other parameters and hence defining the necessary optimum features for porous structures and enabling functional and successful fabrication of parts using Additive manufacturing with superior qualities that IN718 offers.

1.3. Approach

In this study, it is critical to establish a relation between porous structures and their effect on the mechanical properties along with the microstructural characteristics. Hence, preliminary efforts involved conducting an extensive literature review to comprehend: (a) the fundamental characteristics of additively manufactured IN718 parts, (ii) various porous structures used in additive manufacturing (AM), (iii) conventional modes of fabrication used on IN718 parts, (iv) microstructural properties of AM fabricated IN718 parts, (v) mechanical properties of AM- fabricated porous IN718 parts. Designs for several porous structures were laid out on CAD tools. Further, the parts were fabricated on EOS M290 with all the

necessary process parameters considered to obtain parts with stable microstructure and texture. Several Scanning Electron Microscopy (SEM) observations were made to study and record the microstructure of the as-fabricated parts. Next, Mechanical tests were conducted to observe the effects of compression and hardness of the samples. Again, microstructural analysis through SEM was carried out to inspect the specimen post compression to learn the causes for the failure.

1.4. Outline

Chapter 1 provides a synopsis of the work with a briefing on the concepts explored in terms of literature review and processes carried out.

Chapter 2 contains literature review of some of the previous studies conducted on IN718 along with further scopes of research. The second chapter also briefly covers general information about the super alloy such as its history, conventional methods of manufacturing, applications, mechanical and microstructural properties of LPBF fabricated IN718 parts and the porous versions of the same.

Chapter 3 covers the design conception of all the parts considering the end application in research perspective. Further discussions involve powder preparation, fabrication, post processing and other experimental test procedures necessary to obtain mechanical properties (compression, and Hardness) and microstructural analysis such as SEM.

Chapter 4 discusses the results obtained from the proposed work with individual focus on microstructural properties of as-fabricated parts, mechanical properties corresponding to each porous structure along with the microstructural analysis of the rupture regions. Also, further providing a comparison of mechanical properties of each porous structure.

Chapter 5 outlines the conclusion and discussion on further scope and progression in the research.

1.5. Contribution

Following the completion, this work contributes towards:

1. Effect of porous structure on microstructure and mechanical properties.

2. Identifying the relationship between the microstructure features and mechanical properties of LPBF fabricated porous IN718.

1.6. Publications

1. Study on the microstructural and hardness variations of unsupported overhangs fabricated using selective laser melting. Proceedings Volume 11589, Behavior and Mechanics of Multifunctional Materials XV; 115890O (2021) https://doi.org/10.1117/12.2585605

Chapter 2. Background and Literature Review

2.1. Inconel 718 Superalloy

2.1.1. History, Properties, and Applications of IN718

Developed by International Nickel Company in 1959, IN718 is a Nickel based super alloy possessing excellent high temperature, mechanical and metallurgical properties accounting to an innumerable variety of applications [2, 3]. Furthermore, its ability to retain the mechanical, chemical, and metallurgical attributes at high temperatures gives it the classification of a "Superalloy" [3, 4]. Initially in 1906, Monel pioneered the development of IN718 as a corrosion resistant nickel super alloy. Later, in Hereford England, Wiggin Alloys developed the superalloy further to be used in jet engines. Further in 1959, International Company developed it into a strengthened and non-age hardening superalloy. P&W can be credited for introducing the superalloy to the mainstream in 1960. The superalloy exhibits excellent resistance against oxidation and corrosion at high temperatures due to the high level of nickel content (50-55%) [5-9]. The superior blend of the attributes that IN718 possesses (High temperature performance, good creep and fatigue properties, oxidation resistance and superior hardness) enabled its utilization in military (in early 1960s), gas turbines, nuclear, oil and gas and high-performance tooling applications [10].

2.1.2. Chemical Composition

IN718 has been identified as N07718 by the Unified Numbering System (UNS). The super alloy constitutes precipitation hardening Nickel-Chromium along with significant amounts of Iron, Molybdenum, Columbium and contains lesser amounts of Aluminum and Titanium. Nickel and Chromium greatly contribute towards IN718's superior high temperature performance. Also, the presence of Aluminum and Titanium provide good weldability. With a good 17 to 21% of chromium in the alloy, resistance to oxidation is greatly enhanced. Table 1 briefs the elements involved in the amalgamation of the super alloy along with their corresponding composition percentage.

Table 1. Chemical Composition of IN718 [4, 11, 12].

Element	Composition (%)
Aluminum	0.20 to 0.80
Boron	0.006 max
Carbon	0.08 max
Chromium	17 to 21
Cobalt	1.0 max
Copper	0.30 max
Columbium + Tantalum	4.75 to 5.50
Iron	Remainder
Manganese	0.35 max
Molybdenum	2.80 to 0.80
Nickel	50 to 55
Phosphorous	0.015 max
Silicon	0.35 max
Sulphur	0.015 max

The most common phases observed in the alloy are γ, γ', γ", and δ. These phases have a great influence on the microstructure and hence the mechanical properties of the superalloy. These alloying phases comprises precipitates that are formed due to the alloying matrix with other constituent elements. It can be observed that (it) γ' has the composition Ni_3(Al, Ti) and a cubic (L12) crystal structure, (ii) γ″ has composition Ni_3Nb and BCT (D022) crystal structure, and (iii) δ has a composition of Ni_3Nb and an orthorhombic (D0a) crystal structure. Further, it can be observed that local Nb and residual δ particles tend to alter the kinetic nature of the precipitates as it would lead to regulated grain growth. Even in the absence of δ phase particles, precipitates like carbides could provide grain growth inhibition. Table 2 shows the commonly observed phases of IN718 [13].

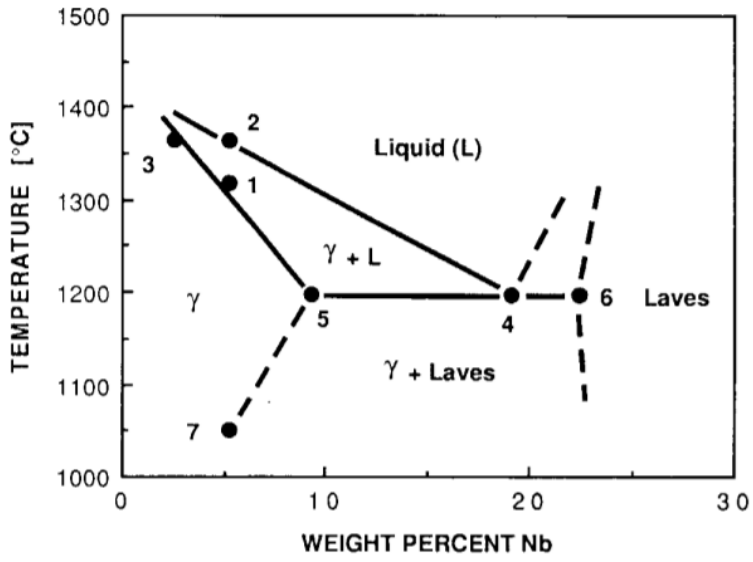

Figure 1: Phase diagram for the solidification of IN718 (Typically for 4.75 to 5.50% of Columbium (or Niobium Nb)[14].

Table 2: Phases of IN718 [15].

Phase	Crystal structure	Chemical formula
γ	Face Centered Cube	Ni
γ'	Face Centered Cube	Ni_3(Al, Ti)
γ"	Body-Centered Tetragonal	Ni_3Nb
δ	Orthorhombic	Ni_3Nb
MC	Cubic	(Nb,Ti)C
Laves	Hexagonal	$(Ni,Fe,Cr)_2(Nb,Mo,Ti)$

2.2. Fabrication of IN718

2.2.1. Conventional Fabrication of IN718

The superalloy IN718 parts can be fabricated through numerous techniques. Each application would depend on the combination of composition, microstructure, and mechanical properties. To obtain attribute and application specific IN718 parts of the highest quality, it is crucial to choose the right form of manufacturing technique along with necessary post processing practices.

Inconel 718 superalloy parts have been manufactured through techniques such as casting, powder metallurgy and wrought processes [16]. One of the oldest methods used for manufacturing IN718 is casting which involves molten liquid poured into a desired mold cavity and then solidified part is removed from the mold. Casting of IN718 results in good grain flow but lacks the necessary grain structure which can be rectified with necessary post processing procedures such as hot isostatic pressing [17]. Sometimes machining would also be required to rectify geometrical accuracy or bring in the necessary finishing. Similarly, wrought processes can be used to obtain wrought IN718 with necessary metallurgical properties. In wrought techniques which is referred to as "worked", hot metal right out of the furnace is subjected to impact and shaped into a desired form. The obtained form is permanent as the part undergoes plastic deformation [18]. The high strength in the case of IN718 greatly limits the possibility of cold working process as it would require a large amount of energy to rearrange the molecular bonds of the super alloy at ambient temperatures.

Alternatively, some of the other potential methods of fabrication include die casting and powder metallurgy [19]. Die-cast IN718 parts tend to exhibit smooth and consistent fatigue features courtesy of well – formed microstructure but this form of phases in microstructure can only be achieved through necessary optimization and refinements in the process. Powder metallurgy on the other hand, is one of the most commonly used methods to fabricate IN718 parts [20]. Powder metallurgy is known to produce parts with high geometrical accurate and near net shaped parts with uniform and refined grain structure. This mode would further require post processing procedures to address the issue of porosity.

Although conventional fabrication methods can be used to fabricate IN718 parts, there are diverse limitations and drawbacks associated with each technique. For example, some techniques involving post processing such as heat treatment could lead to oxides hence reducing the ductility at high temperatures [21, 22]. Some of these problems associated to conventional manufacturing techniques can be dealt with using Additive manufacturing methods such as Direct Energy Deposition (DED) and Laser Powder Bed Fusion (LPBF) [23, 24].


Figure 2: IN718 fabrication through conventional methods of casting [25] and Wrought process [26].

The IN718 parts fabricated through conventional means require a series of postprocessing procedures to achieve desired geometrical, metallurgical, and mechanical attributes. In the initial phase the part undergoes necessary mechanical processing to facilitate necessary finishing for the part. Typically, the machining process yields best results when the metal is softer and has the least resistance to machining processes as it exists in its annealed and stress relieved state of condition and is further followed by final aging processes. The aging processes are performed on the parts to enhance hardness and strength [15].

The final postprocessing procedure the parts undergo would be the heat treatments. Using heat treatments, the mechanical and chemical properties along with the microstructural conditions can be modified through controlled cycles of heating and cooling. Typically, these processes are performed at a temperature high enough to facilitate thermal diffusion but lower than the melting point of the material used. IN718 parts would generally require heat treatments such as hot isostatic pressing (HIP), annealing and alternate cycles of cooling, and aging depending on the desired microstructure [15].

Annealing is a process in which the part is subjected to high temperature to initiate recrystallization of the grains hence gradually relieving the residual and thermal stresses accumulated during the fabrication process (cold/hot worked and casting) and promoting homogeneity of the alloying constituents. At a controlled temperature below the melting point, high enough to create necessary diffusion, recrystallization gradually develops in the material and further creates a conducive condition for grain growth. Annealing,

at specific temperatures also dissolves precipitates through a process called 'solution annealing'. Solution annealing depending on the corrosive nature of the material, involves the use of water, brine, or polymer-based solutions. The solution annealing and homogenization process for IN718 parts may typically take up to 4 hours [15].

As explored earlier, Hot Isostatic Pressing (HIP) is required to improve the density of parts fabricated using powder metallurgy or casting [27]. This process uses a combination of high temperature and pressure to reduce the porosity of parts fabricated through casting and can be used for AM fabricated IN718 parts as well. Necessary pressure is uniformly applied on the parts with a temperature high enough to begin diffusion, this helps by either closing the pores or significantly reducing the size of the pores and hence reducing the overall porosity of the parts [28].

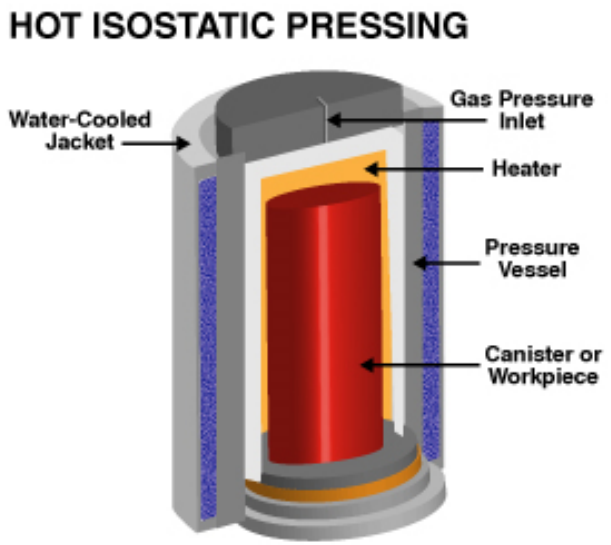

Figure 3: Schematic of Hot Isostatic Pressing [28].

Aging or Age Hardening is a process used to induce hardness and strength into the fabricated parts through the means of thermal activity of intermediate temperature ranges that create necessary conditions for the formation of secondary phases of the microstructure of the alloy. Age hardening process is sometimes also referred to as the precipitation hardening process as precipitation of intermetallic compounds occur during these intermediate temperatures. Further, Cooling process is a crucial step to be

carried out to gradually slow down or completely halt the recrystallization process when the right phases and crystal structures have been achieved at a particular temperature. Fluids such as Water, Oil, inert gases such as argon, nitrogen and helium can be used to provide necessary cooling of the parts. Both annealing and cooling processes are critical to parts fabricated using casting and wrought methods to develop the right hardness and strength [15].

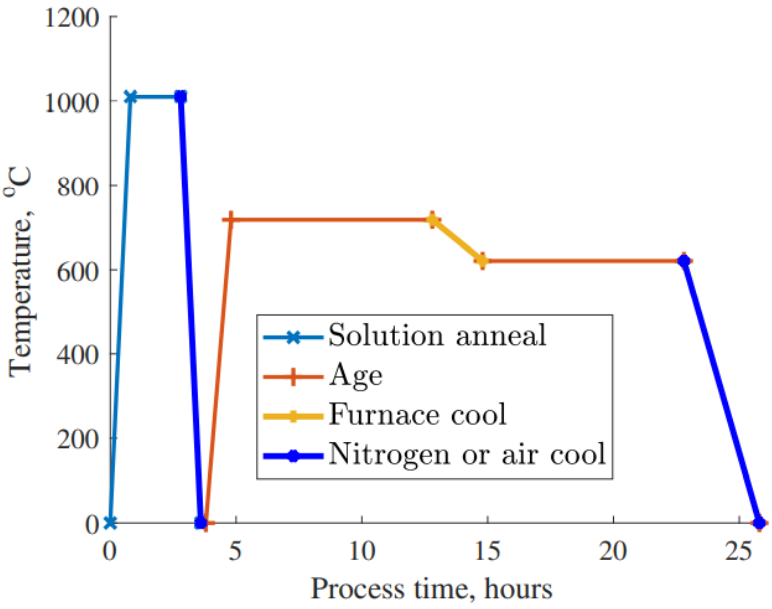

Figure 4: Graphical representation of heat treatment processes required for IN718 [15].

2.2.2. Metal Additive Manufacturing

Additive manufacturing technique is relatively a new technology which was initially used to fabricate functional prototypes [29-32]. Additive manufacturing involves dynamic stacking of successive layers to produce the shape of a desired part [33-37]. With progressive research carried out over time, AM has evolved into a mainstream mode of fabrication [38-40]. AM permits a wide variety of metallic, non-metallic, ceramic, and plastic based materials that can be used for fabrication [41-47]. Although AM techniques could prove to be advantageous over conventional methods, there still exist several drawbacks.

Some of the advantages include economical and small batch production, consolidation of an assembly into lesser number of parts, porous structures can be incorporated, complex designs with internal features can be fabricated with ease [48-53]. GE aviation in collaboration with Morris Technologies in 2012 tested the limitations of AM, as a result the engineers were able integrate 20 different parts of a jet engine fuel nozzle into a single component hence cutting down on assembly time and reducing overall weight by 25%. Similarly, in GE's advanced turboprop engine a total of 855 parts were reduced to just 12 components with the help of Additive manufacturing [54]. Among the various advantages of AM, "printing on demand" is a significant ability that cannot be achieved through conventional methods. In 2014, NASA contracted 'Made In Space Inc.' to design a ratchet and several wrenches. 3D CAD models were transmitted to the International Space Station and was successfully fabricated on the on-board 3D printer [55].

Figure 5: A ratchet wrench fabricated onboard the ISS using AM [55].

Metal additive manufacturing is one of the classifications of additive manufacturing, as the name suggests metal parts are fabricated using AM techniques. Some of the examples of metal additive manufacturing includes, Selective Laser Melting (SLS), Direct Energy Deposition (DED), Electron Beam Melting (EBM), Direct Metal Laser Sintering (DMLS), and Laser cusing. Figure 8 denotes a detailed classification of Metal additive manufacturing techniques currently in practice.

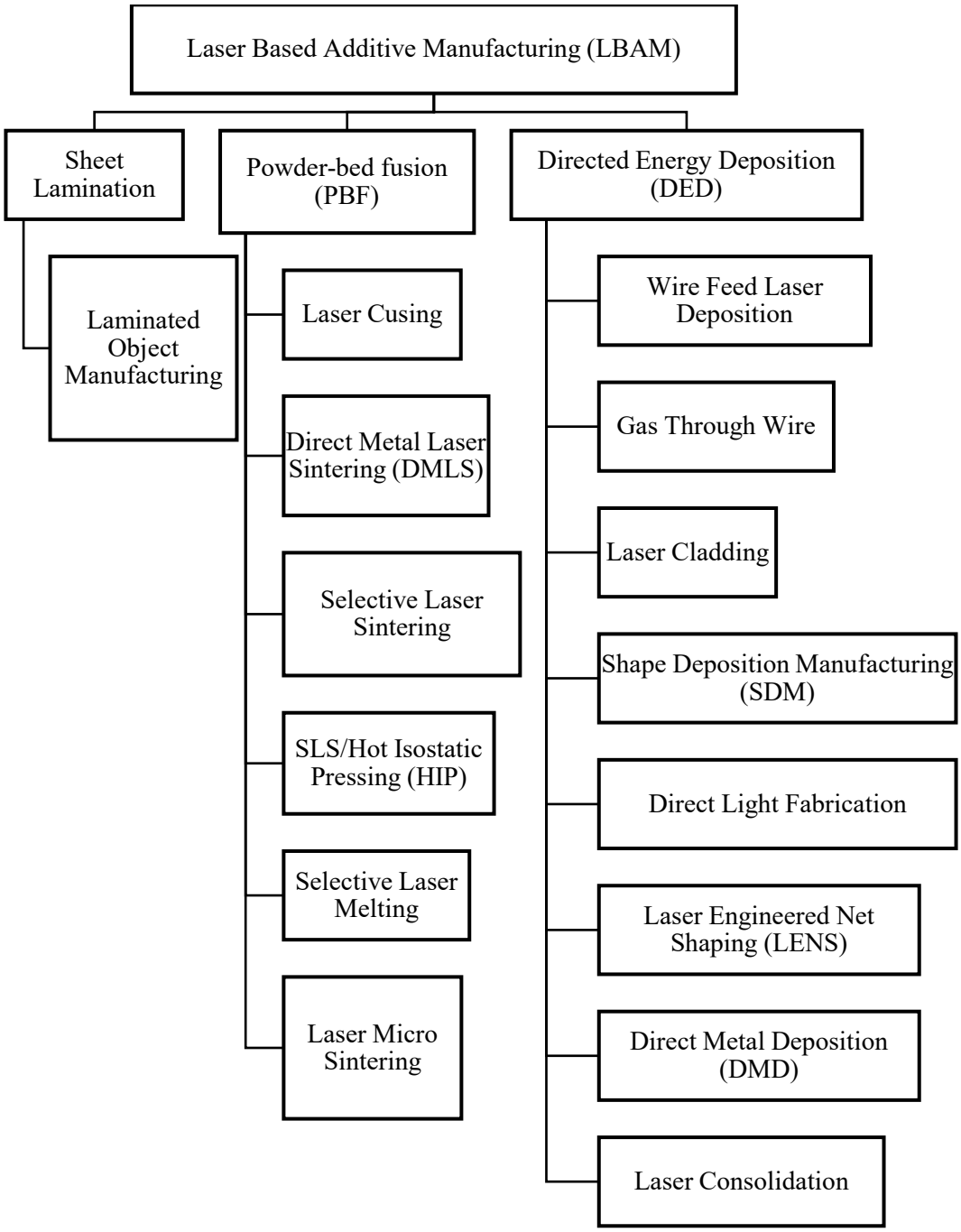

Figure 6: Classification of Metal Additive Manufacturing techniques.

Metal additive manufacturing has seen a dramatic development over a period of 3 decades. Researchers Deckard and Beaman are credited for their pioneering efforts to create the first metal 3D printing system at the University of Texas at Austin. Their initial efforts involved creating a 3D part from

metal powder with the help of a YAG laser bearing 100W of power as a heat source. The initial trials were made on polymers and then proceeded further to metals. With a limited success rate, in 1986 there was a shift of focus to fabricate of Polymer parts, for which SLS was to be developed. Deckard and Beaman went on to naming this project the 'Betsy' which also included the first ever automated system aimed at powder distribution. This further led to the patent of SLS at the University of Texas at Austin in 1986. However, SLS has also been presently used for metals as well and the boundaries of sintering further pushed to SLM or Selective Laser Melting license credited to EOS GmbH. Later in 1989, Inkjet binder deposition-based AM process was patented as "Three – Dimensional Printing" at MIT. Inkjet binder deposition process is now commonly known as Binder Jetting and the word "3D printing" has become synonymous to all forms of additive manufacturing. The same process with necessary binders used, can now be seen for the fabrication of metal parts. Sandia National Laboratories, in 1995 explored and modified the idea of wire feedstock based Direct Energy Deposition (DED) technique using a laser heat source on powder feedstock instead to introduce the first commercial machine with the trademark of Laser Engineered Net Shaping (LENS). Later in 2000, with extensive research made on Electron Beam Melting or EBM, Arcam AB held the licensing rights for the process post acquisition of its patent credited to Andersson & Larson made from Sweden. While Arcam launched its first ever EBM machine in 2002, 3D system acquired the rights for SLS in 2001 by purchasing the company which held Deckard's original patents. Recent advancements include the certification of implants for medical applications. CE certified the first hip implant fabricated using EBM technology in 2007[56]. On the other hand, in 1999 Fockele and Schwarze (F&S) introduced the first SLM system in Germany. Later in 2004, F&S partnered with MTT Technologies group (then known as MCP) to release the first commercial SLM machine, the MCP Realizer 250 [57]. Some of the other notable benchmarks in the history of metal additive manufacturing can be observed in the figure 6 below.

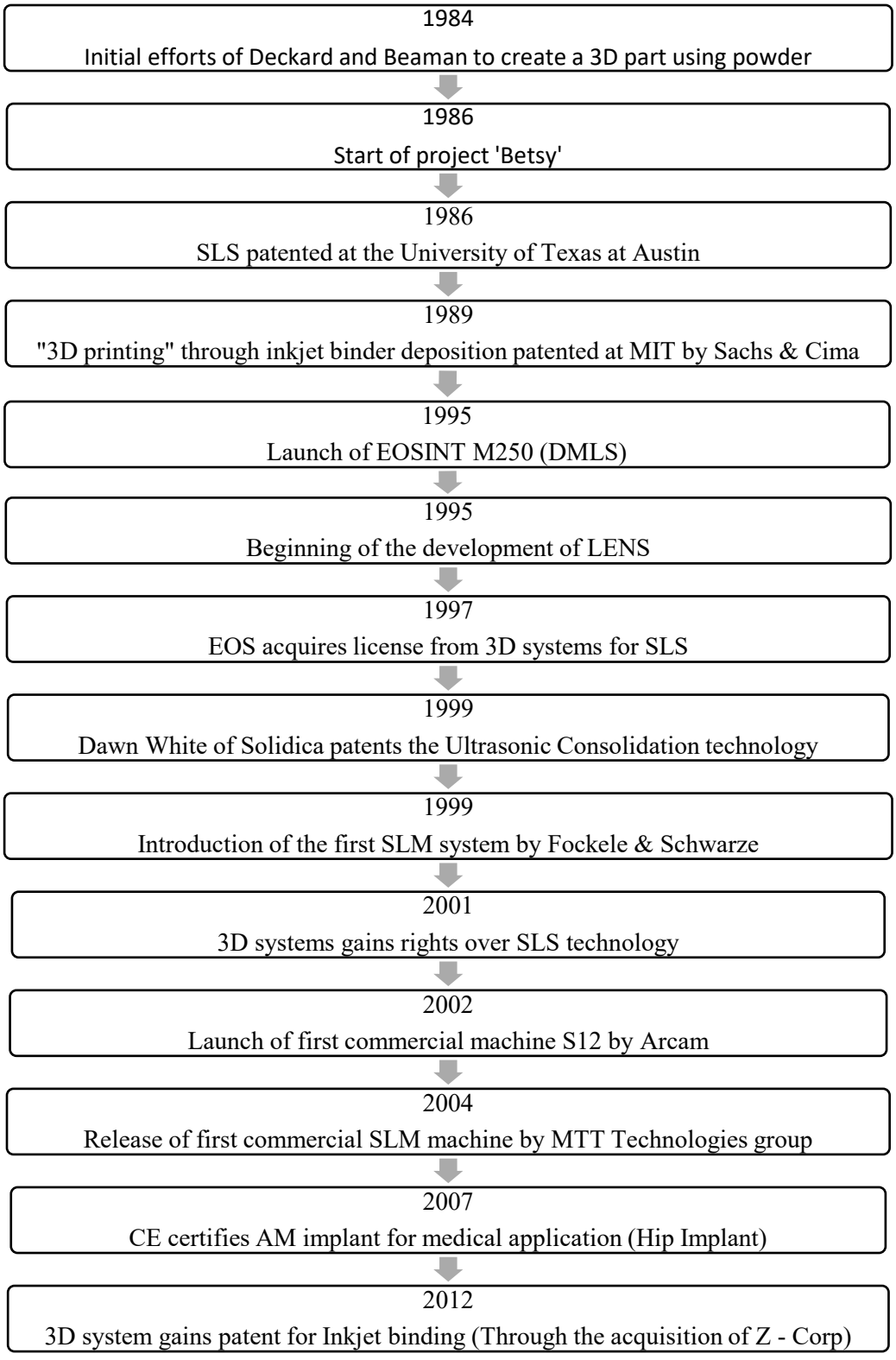

Figure 7: Brief history of Metal Additive Manufacturing [56, 57].

With various methods of metal additive manufacturing available, the most suitable technique used for the fabrication of IN718 is Powder-Bed based Fusion (PBF) classified under Laser based additive manufacturing (LBAM) techniques [58, 59]. PBF fabrication promises high geometrical accuracy while enabling fast process for durable and functional parts. The process also introduces the possibility of implementing overhangs up to 45 degrees from the horizontal plane, further also permits complex geometries, chemical resistance properties, high strength and stiffness, while nesting of multiple parts into a single print bed is also enabled [60, 61].

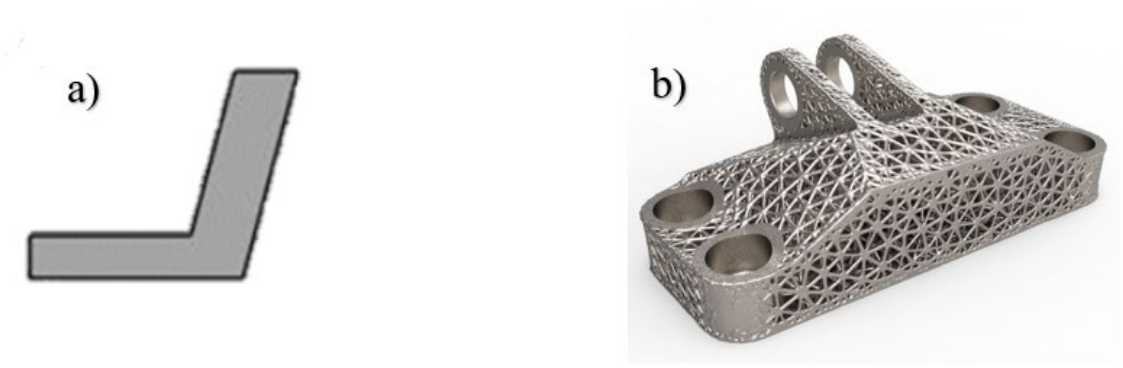

Figure 8: a) Overhangs [62] and b) complex geometry fabricated using AM techniques [63].

Selective Laser Melting is a Metal AM technique which evolved from SLS, both require the use of fiber laser technology as a heating source. SLM uses the laser heat source to selectively melt adjacent metal powder particles and combine them to form a solid part [57]. Like various other AM processes, SLM builds parts by selectively melting successive layers of the CAD file fed into the fabricating system. One of the main notable capability of SLM is, the manufactured parts exhibit beyond satisfactory or acceptable range of mechanical and microstructural attributes and further, as – fabricated parts are fully functional and can be directly utilized for its intended application.

SLM process involves a powder deposition system consisting of a recoater and a roller that deposits a uniform layer of material on the printing substrate. With each successive layer subjected laser scanning and solidification, the substrate moves down. The displacement of each downward movement of the layer

is the same as the layer thickness of the part being fabricated [64]. The process also negates the possibility of oxidation as the build chamber is filled with inert gases such as argon during fabrication.

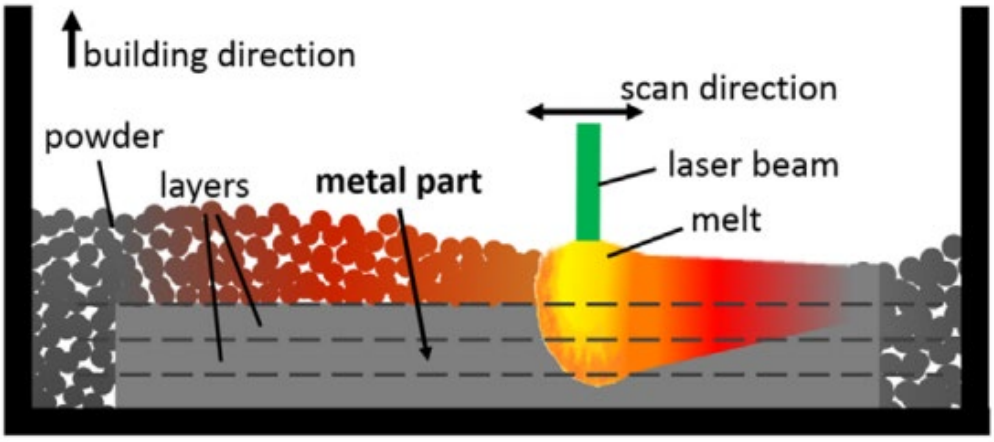

Figure 9: Part fabrication using SLM [65].

Both SLM and SLS classified under PBF form of additive manufacturing require feedstock of metal and alloys in their powdered form. It is critically essential to carefully consider characteristics such as chemical composition, powder morphology, particle size range, density, angle of repose and flowability for the powder to be eligible for the fabrication process. The powder metallurgical process to produce metal powders vary for each metal or corresponding alloys. A general classification of the wide range of powder metallurgy processes is depicted in the figure 10 below. Mechanical mode of powder manufacturing can be done through process like ball or hammer milling which works best on brittle materials. Ferroalloys and intermetallic powders are commonly produced using these techniques. Whereas metals such as titanium can be processed through Hydride – Dehydride approach. Electrolysis powder processing techniques are based on the principle of electroplating and can be used on electrolytic materials like copper. Similarly chemical mode can be used to obtain Iron or Nickel powders using carbonyl process, thermal decomposition techniques can be used to obtain powders for materials like Platinum. Finally, Atomization is the most used method to produce metal powders as it can be used on a wide range of materials while providing a consistent

sphericity of the particles and has an excellent production rate. In this process, molten metal is atomized to form fine powdered particles. The atomization process can be classified into air atomization, inert gas atomization, water atomization, and Electron Induction gas atomization among the other classifications.

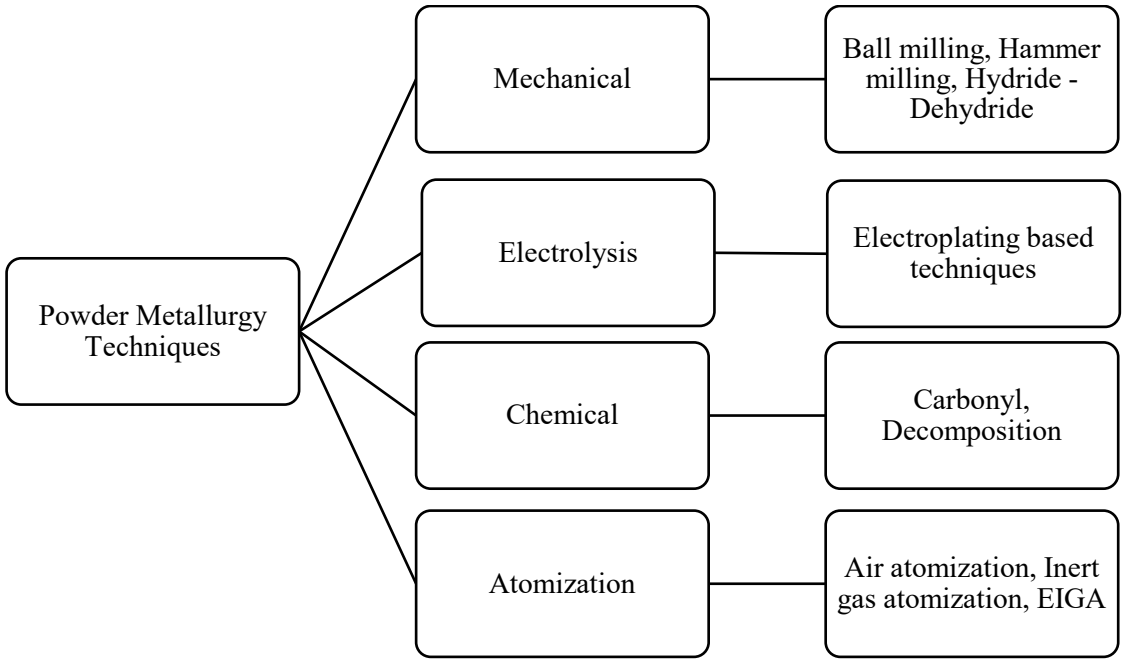

Figure 10: Powder Metallurgy techniques used to produce metal and alloy powders.

Some LPBF processes require the use of additives to create necessary bonds between the powdered particles and may further require chemical based postprocessing to complete the binding. However, SLM eliminates the necessity of intermediate binding agents for fabrication of metals hence eliminating the need for further postprocessing activities [66]. While providing an economical and efficient use of materials, SLM also enables recycling of unused powder with no toxic chemicals involved in the process. Further, the obscurity of oxidation occurring in the process ensures homogeneity of alloying elements which significantly influence the mechanical attributes of the fabricated part. Considering these abilities, SLM poses paramount advantage in comparison to the conventional counterparts.

Processing parameters play a major role in successful fabrication of SLM parts. These parameters primarily tend to affect porosity, geometrical accuracy, grain structure and hence observable phases. The

changes in parameters could also be directly linked to the degree of defects that can form during the fabrication process [67]. Ravichander et. al., studied the effects of process parameters in PBF on as – fabricated IN718 parts. They established the effect of scan speed on the geometrical accuracy, grain growth, percentage of γ" phases and epitaxial bonding. Also, hatch spacing affects the hardness of the as – fabricated parts [64, 68].

Contrary to the advantageous aspects, SLM also exhibits certain drawbacks. The manufacturing cost in comparison to the conventional methods is high due to the use of metal powders. It is of significant necessity to use metal powder of the right morphology, particle size, and negligible percentage of impurities. Further, fabrication time to process small quantity of material is high but this can be optimized by introducing periodic cellular lattice structures. With introduction of these structures, the amount of material is reduced hence reducing the energy consumption and overall build time. The cooling rates of around 106K/s which is typically high induces residual thermal stresses and dislocation densities. Also, recycled powder tends to display altered mechanical properties which further affects the mechanical attributes of the final part [69, 70].

SLM like other manufacturing process, regardless of conventional and additive manufacturing processes has its share of drawbacks and limitations. While some of the limitations and drawbacks have been explored earlier, defects tend to deprive the desired range of mechanical properties of as – fabricated parts. Some of the major defects observed in SLM fabricated parts are Porosity, cracks, unmelted powder, surface quality, and anisotropy among other defects. The root cause of each of these defects can be traced back to the process parameters, material, thermal and chemical properties of the metal used for fabrication, impurities, and ambient conditions. Galy et. al., studied the common defect in SLM fabricated aluminum alloys and enlisted various causes for each of the defects. The study focused mainly on four forms of defects namely porosity, hot cracking, anisotropy, and surface quality [71]. Porosity being considered one of the most critical defects, determines the overall quality of the part in terms of tensile and compressive strengths. Also, depending on the size of the pores, categorized as micropores and macropores lack of sphericity could

lead to cracks rendering fragility to the entire fabricated part [71, 72]. Anisotropy on the other hand is of lesser significance compared to porous defects. This defect usually is a result of complex thermal history and build orientation could also contribute to the cause. Anisotropy could cause non uniform range of mechanical properties across SLM fabricated parts. Similarly unmelted powder caused due to insufficient laser power or high scan speeds has adverse effects on the mechanical properties [72].

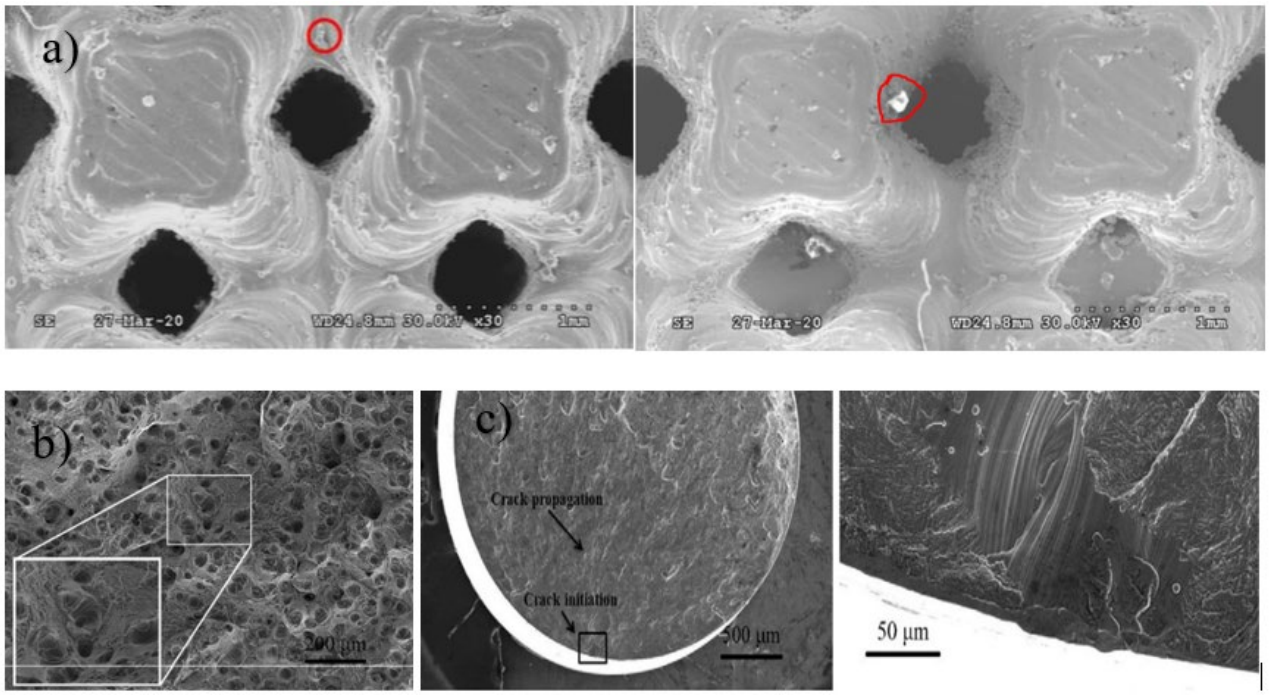

Figure 11: SEM images of a) partially/unmelted powder [73, 74], b) pores and c) cracks [72].

Over the last few years, Inconel 718 has been broadly fabricated using Laser-based additive manufacturing techniques. Limitations of conventional fabrication methods used for IN718 have been overcome using LBAM while still maintaining its superior mechanical attributes. Though LBAM can be widely classified into processes such as Directed Energy Deposition (DED), Powder Bed Fusion (PBF), and Sheet Lamination; PBF has been extensively used for the fabrication of IN718 components. PBF processes facilitate fabrication in a shorter time compared to other LBAM techniques while also providing a greater geometrical accuracy. PBF also permits a greater flexibility in introducing complex geometries, overhang angles, and inducing good strength and stiffness into the design of the IN718 parts [62].

Some of the PBF techniques that can be used for the fabrication of IN718 parts are Selective Laser Sintering (SLS), Selective Laser Melting (SLM) and Direct Metal Laser Sintering (DMLS). Both SLM and SLS have similar preprocessing inputs via sliced CAD files but the input parameters are of a higher magnitude for SLM to ensure melting of powder particles. SLM requires a careful choice of optimized processing parameters to obtain desired quality of print [60]. In comparison, SLM produces up to 100% dense parts and is consumer ready while SLS is widely used for rapid prototyping and productions of low batch sizes [60, 75]. Also, parts fabricated using DMLS tend to be void on internal defects while also evading balling phenomenon [76, 77].

Selective Laser Sintering (SLS) commonly used for purposes of rapid prototyping, is a PBF based technique which uses high powered laser as a heat source to partially sinter powder particles to ensure binding of the material. Unlike SLM, the level of powder melting in SLS is comparatively low due to which the fabricated parts are usually porous and hence reducing the overall density of the part. An evident observation of porous surfaces can also be seen in SLS fabricated parts. With the level of porosity and low density, the mechanical property of the fabricated part is significantly compromised. The porosity levels can be reduced through postprocessing procedures such as Hot Isostatic Pressing (HIP) or cyanoacrylate coatings over the fabricated part. Considering the same material, SLM parts tend to exhibit better levels of porosity and promising mechanical properties when compared to parts fabricated through SLS [78].

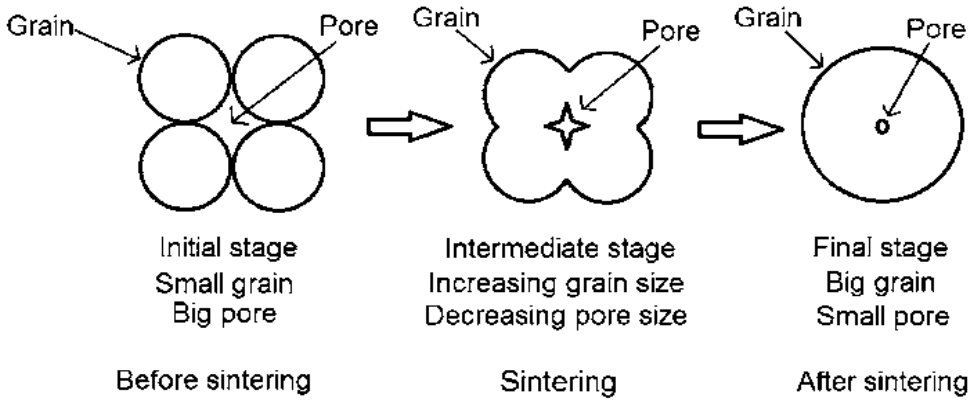

Figure 12: A simple model of sintering process [79].

DMLS or Direct Metal Laser Sintering is also a LBAM process classified under PBF Technique. This process can be used on a single metal powder consisting of two different grain sizes and shapes to form a part. The process involves successive cycles of complete sintering of a powder layer which may include the cross section of both the supports and the part itself followed by recoating of the next powder layer. This process completely negates the possibility of balling phenomenon and can also produce parts with any internal defects [76, 77].

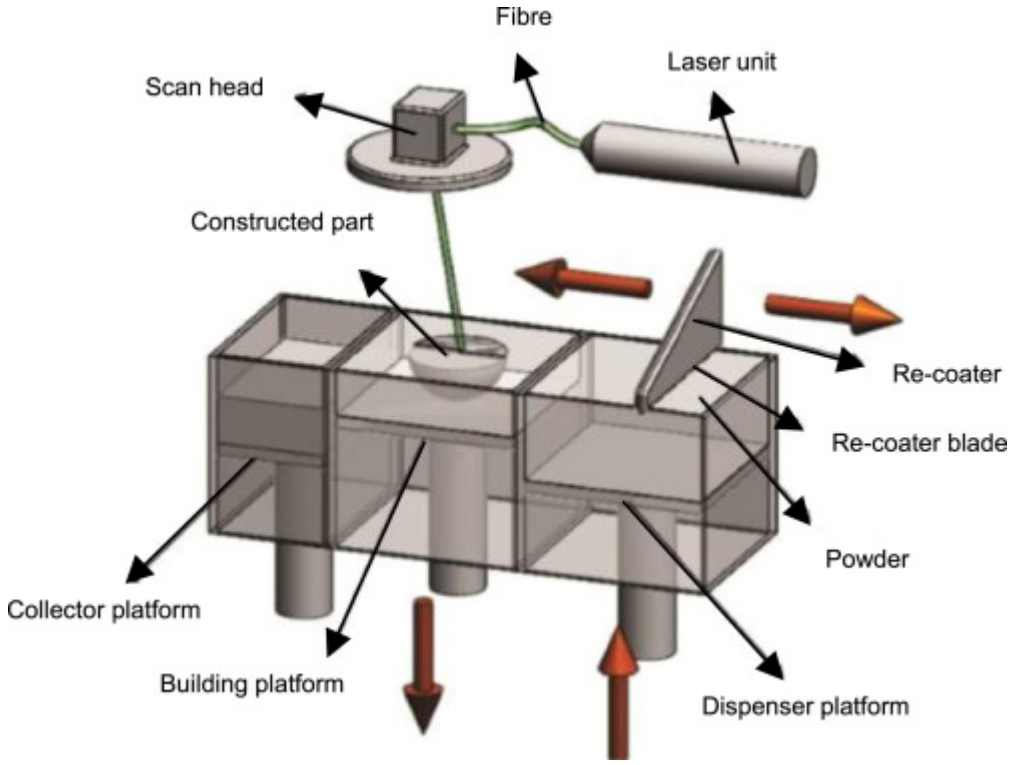

Figure 13: Schematic representation of a DMLS system [80].

2.2.3. Additive Manufacturing of Porous IN718

Although porous topologies were introduced more than a century ago, implementing them into conventional manufacturing technique has been quite limited due to the complex nature of their geometries. These limitations can be surpassed with the current advancements in manufacturing techniques [81]. Also, the size and shapes of the pores can be further regulated with controlled processing parameters.

Additive manufacturing greatly enables the implementation of porous materials and in the case of metals, LBAM is a reliable technology. Among LBAM techniques, SLM provides high geometrical accuracy and resolution which would make it the best option for the fabrication of porous IN718 parts [82].

The use of support structures is a common practice in additive manufacturing. But some complex structures can be fabricated without the use of support structures and gyroid structure can be considered as a typical example. A gyroid unit cell is typically composed of smooth struts with a spherical core and circular cross section. With each progressive layer, the inclination angle of the circular struts varies creating a gradual growth with changing area and position. This makes the gyroid structures self-supporting by supporting adjacent layers during SLM process [83].

With most prominent process parameters being the scan speed, laser power, layer thickness and hatch spacing choosing the optimum magnitudes can help altering the microstructure and mechanical properties of other LBAM techniques as desired since compared to SLM, other LBAM techniques tend to exhibit vastly varying attributes in the manufactured final part. Considering the mentioned parameters, the key is to obtain the right energy density. Energy density can be evaluated using the following expression:

$$E = \frac{p}{h * v * t} \qquad \text{Equation 1}$$

Where, E – energy density, P – laser power, h – hatching space, v – scan speed, t – layer thickness [64, 84-86]

2.3. Porous IN718 Structures

The most distinct features of cellular structure include reduced weight, good resilience to impact loads, excellent acoustic, and thermal insulation [53, 87]. The cellular structures can be classified into periodic and stochastic structures. Stochastic porous structures, as the name suggests is a random arrangement of voids whereas periodic porous structures are uniformly structured and recurring pattern of voids. Honeycombs, lattice structures exemplify periodic porous structures.

Among the classification, periodic porous structures tend to demonstrate superior mechanical properties such as stiffness and strength. Periodic structures offer flexibility in designing to facilitate

necessary range of mechanical attributes such as loading capacities and improved surface area depending on the type of applications [88]. This versatile nature of periodic porous structures makes it suitable for multifunctional performance-based products in automobile, aerospace, and other such applications.

2.3.1. Lattice Structures

Lattice periodic cellular/porous structures are typically characterized by organized arrangement of open pores called unit cells. The unit cell based mechanical behavior such as tensile and compression properties tend to be superior to that of stochastic. Mechanical properties can be altered to requirement by regulating the geometry and the topology of the cell. For lattice structures, the unit cells are classified by their deformation behavior and formation.

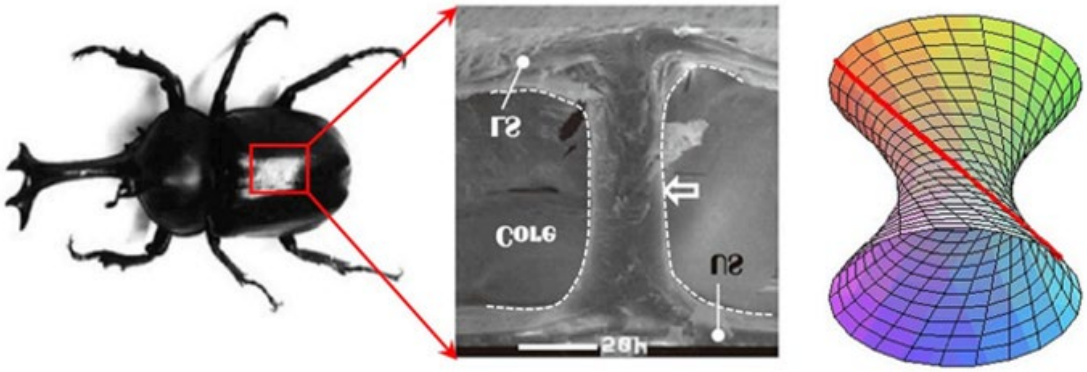

Figure 14: Cylindrical tube microstructure observed in the front wing of an adult allomyrina dichotoma beetle [89].

The major inspiration for the design of commonly used porous structures is derived from molecular structures, and naturally occurring patterns of structures as can be observed in the figure above. Some of the examples of lattice structures are honeycomb, BCC, FCC, BCC-Z. [90].The nomenclature given for the lattice structure are based on crystal structures and vertical struts are denoted by Z. BCC, FCC, BCC-Z and FCC-Z along with other similar lattice structures are further classified as Stretch-dominated lattice structures which exhibit good attributes such as strength and stiffness and Bending-dominated lattice structures display characteristics such as specific resilience for high stress plateau under compression [91].

Nature inspired Honeycomb structures are prismatic and tend to exhibit good and stable resistance to definite loads and flows however the thin walls tend to fail under lateral strength and stiffness. Certain modifications made to the honeycomb structure would result in a structure called sandwich panels to improve resistance to lateral loads.

Similarly, having received a significant attention, Body-Centered cubic structure or BCC displays a bending dominated nature hence possessing excellent energy absorbing performance and mechanical strength [92-95]. Also, FCC-Z and BCC-Z credit to Leary et al. seem to exhibit high compressive strength and stiffness along the Z-axis struts [96].

Figure 15: Unit cells of a) BCC, b) FCC, c) BCC-Z, and d) FCC-Z [97].

Contrary to the advantages that lattice structures offer with SLM technology, a study conducted by Sienkiewicz et al., suggests that the geometrical accuracy is moderately inaccurate in the direction perpendicular to the material deposition and the side planes resulting in slight 'waviness'. A slight variation was also prominently observed in the strut cross section along the side planes. Further, on performing CT scans, defects typical to metal additive manufacturing such as voids and unmelted powder was evident but was negligible in effect under static tests [98].

2.3.2. Triply Periodic Minimal Surfaces

Derived from naturally occurring microstructures such as cell membranes, equipotential surfaces observed in crystals and block copolymers [99-101], Triply Periodic Minimal Surfaces or TPMS are

Symmetric and crystallographic structures placed under rank-3 lattice of translations. Tetragonal, Orthorhombic and Cubic are some of the examples of TPMS while structures like triclinic and monoclinic structures are difficult to parametrize. Hermann Schwarz in 1865 described the early examples of TPMS [102]. Later, Alan Schoen identified several new TPMS structures based on crystallographic cell based skeleton graphs but failed to produce a mathematical representation which was later presented by Hermann Karcher in 1989 [103, 104]. Many new such structures were found using conjugate surfaces.

The TPMS structures in comparison with the primary forms such as FCC, BCC, etc., tend to exhibit enhanced mechanical properties and structural stability. A study conducted by Lei Zhang et al., on the energy absorption characteristics of TPMS structures was concluded with a comprehensive result on the superiority of TPMS structures in comparison with the BCC structure. In this study, for 316L stainless steel three variants of TPMS structures namely, Primitive(P), Diamond(D), and Gyroid(G) were compared with a simple BCC structure. It was observed that the mechanical properties of TPMS structures were significantly higher than that of the BCC structure and out of which D-type structure displayed the best characteristics with enhanced stiffness, energy absorption ability and plateau stress [105]. A similar study was conducted by Zhao et al. with Ti-6Al-4V and observed a similar result of enhanced mechanical properties and energy absorption [106].

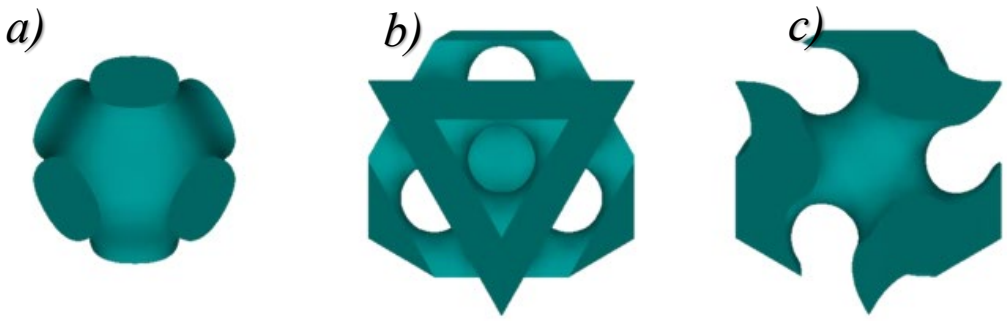

Figure 16: TPMS unit cells of a) Schwarz, b) Diamond, and c) Gyroid structures [83].

2.4. Mechanical Properties

Mechanical properties are influenced by several factors such as cellular patterns, degree of porosity, strut loading response (stretch/bending dominated). While attributes such as compressive strength and young's modulus are primarily in focus, optimum process parameters and build orientation can be regulated to obtain the desired mechanical properties [90, 96, 107]. This section briefly details the influence of porous structures on mechanical properties.

Several studies have been conducted to learn the effects of porous structures on mechanical properties. Lattice performance of FCC, BCC, FCC-Z, BCC-Z under uniaxial compression for AlSi12Mg conducted by Leary et al. demonstrated a large collapse stress to plateau stress ratio [96]. Compressive tests performed on Ti4Al6V with various cellular structures carried out by Sing et al. demonstrated the effect of process parameters on mechanical properties along with the range of elasticity of lattice structures [108]. Similarly, Xiao et al. studied lattice structure performance of 316L stainless steel particularly for FCC, VC and ECC structures and concluded that the increase in porosity levels diminishes the mechanical properties [109].

A study was conducted by Wauthle et al., to understand the static behavior of five titanium lattice structures fabricated in differing build directions. They concluded that compressive strength of vertical and horizontally oriented samples showed similar properties and proved to be up to 35% more superior to that of diagonally oriented sample [110]. Similar experiments were performed by Maskery et al. on Al-Si10-Mg BCC structure. Instron 5969 UTM was used to conduct uniaxial compression tests on the sample. They observed almost a 95% loss of structure at 9% strain rate. Further struts began to display brittle rupture after a brief transition from linear to non-linear elastic behavior. It was then concluded that, even at an increased strain of 50% the structure failed to regain its original strength prior to collapsing [111].

On a similar note, Srivathsan et. al., [73] presented a study on the strength of various porous structures fabricated using SLM. The experiment involved compression tests performed on each of the samples to observe the mechanical behavior of each porosity type. Among the lattice structures, BCC and FCC displayed a good resistance against lateral strain but lacked in strength whereas BCC – Z and FCC – Z

compensated in strength due to the Z – pillar working against the compressive loads but lacked the necessary modulus of elasticity. Among the TPMS structures, Diamond and Schwarz had the least yield points even when compared to the lattice structures but displayed the highest elongation. Their study was also backed by finite element analysis carried on all the porosity types. A comparison was then drawn between simulation and the actual experimentation. An image below shows the results from Ansys analysis.

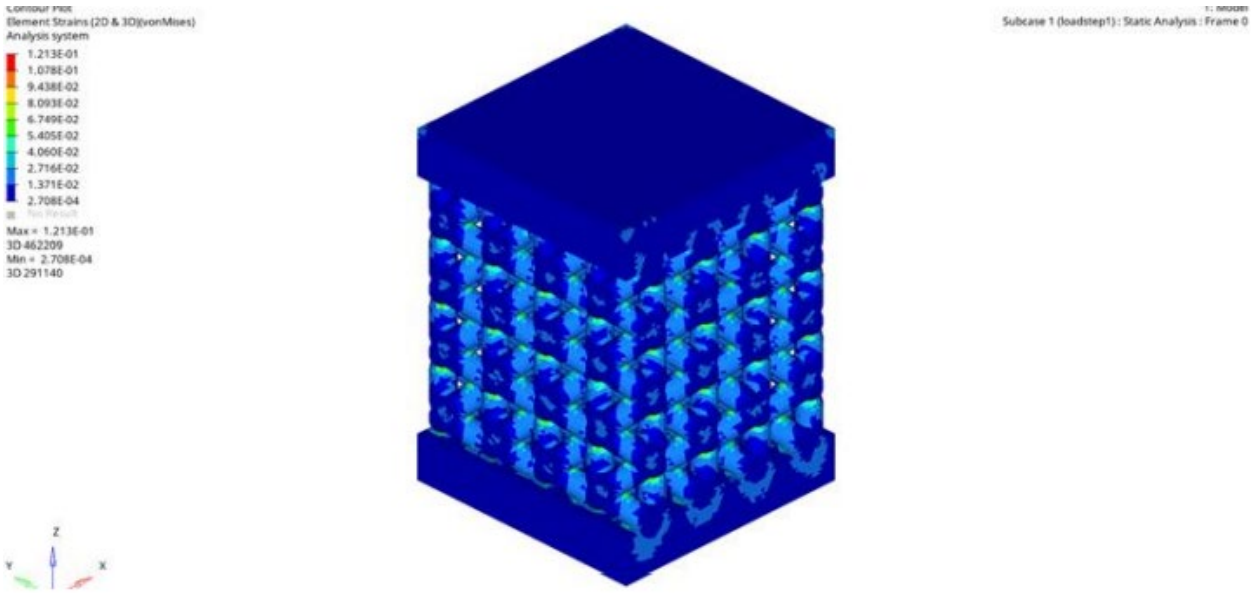

Figure 17: Finite Element Analysis simulation performed on BCC structure [73].

2.5.Microstructural Analysis

Microstructural analysis is necessary to identify the defects that parts with lattice structures fabricated using SLM tend to exhibit. Identification and studying the defects helps in understanding the cause of failure hence enabling adequate control or further ability to eliminate the defects through adapting suitable process parameters [112]. These avoidable defects are usually geometrical defects, internal defects, and residual stresses that could impact the quality of necessary dimensional accuracy, surface roughness or other mechanical attributes and manufacturability. Some of the common defects include residual stresses caused by difference in thermal gradients; voids, un8melted powder, cracks, staircase effect caused by unregulated process parameters [110, 113-115].

Some of the literary work identified the significance of microstructural analysis. Studies on struts of Ti-6Al-4V SLM parts of various lattice structures carried out by Choy et al. noted the geometrical accuracy is dependent on the powder adhesion. Further detailing on how powder adhesion is greater in horizontal struts in comparison with the diagonal struts was stated in this work. The authors also studied the dependency of strut size with respect to geometrical accuracy and concluded that the geometrical accuracy is inferior in smaller diameter of the struts [116]. Similarly, Yan et al. based their study on the balling effect of partially molten powder in stainless steel SLM parts leading to geometrical inaccuracies along with several other defects [82].Studies carried out by Mckown et al., Pattanayak et al., Gangireddy et al. and several other authors mainly focused on cracks caused due to elevated residual stresses and/or rapid cooling [117-119].

Qiu et al. studied the influence of laser power on diamond type lattice of AlSi10Mg. 150W and 400W laser powers were used to fabricate the samples. SEM micrographs and strut diameters were observed, and they concluded a linear relationship between laser power and strut diameter, i.e., greater laser power resulted in thicker struts. They also observed increase in partially melted powder adhering to strut surfaces with increase in laser power. This study can be used to optimize the process parameters, particularly laser power to facilitate a better geometrical accuracy [120].

Patrick Köhnen et al. studied the microstructure of SLM fabricated F2BCC porosity type stainless steel specimens. They observed that the height of the melting tracks caused by epitaxial growth did not inhibit overall grain growth. Most of the grains were observed to be columnar grains with an elongation of a high aspect ratio (greater than 200mm) [121].

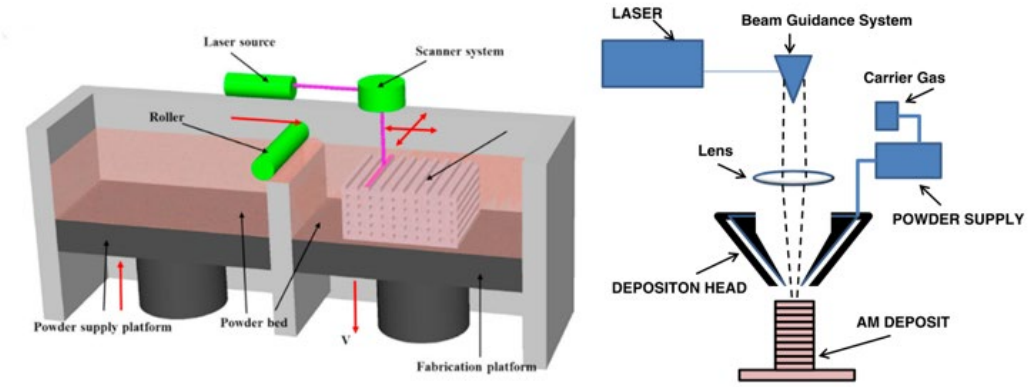

Figure 18: Schematic representation of powder-bed based[122] and flow-based Additive Manufacturing techniques [123].

Chapter 3. Materials and Methods

This chapter outlines the stages of fabrication along with processes necessary before and after the fabrication process. Details of CAD design, powder preparation, IN718 parts fabrication and sample preparation necessary for material and microstructural analysis and post processing procedures are covered in this study.

3.1. CAD design

The study involved the use several lattice structures such as BCC, BCC-Z, FCC, FCC-Z, and TPMS structures namely, Schwarz, Gyroid and diamond models designed with 45% level of porosity to determine the influence of porosity on mechanical properties of IN718 parts fabricated using SLM process.

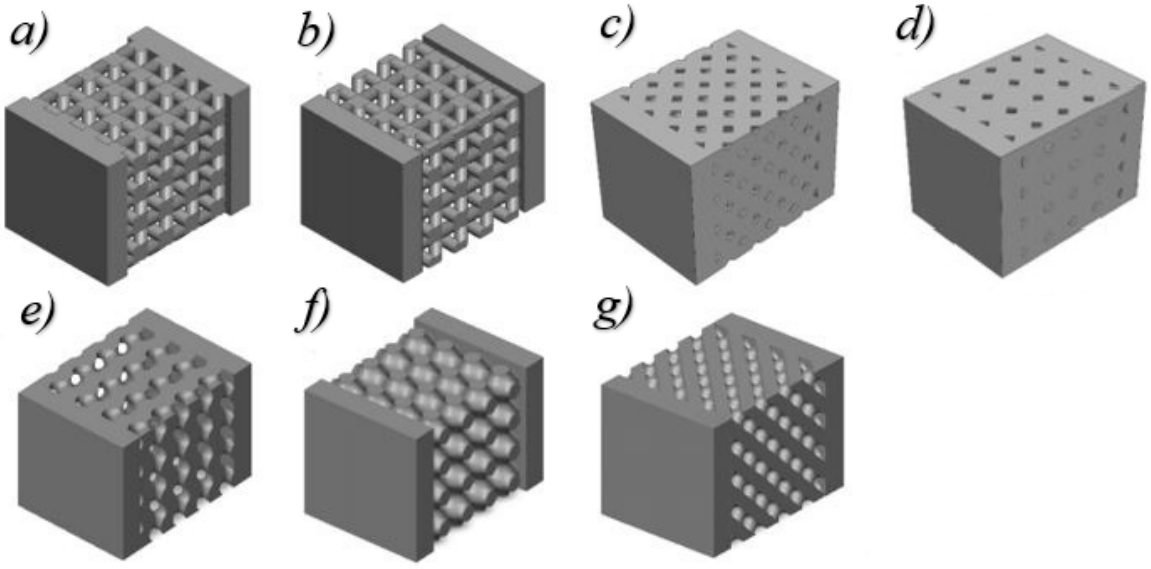

Figure 19: CAD designs of porous structures with 45% porosity: a) , b) BCC-Z, c) FCC, d)FCC-Z, e) Gyroid, f) Schwarz, and g) Diamond.

3.2. Periodic Porous Structures- Lattice Structures

The Lattice structures (BCC, BCC-Z, FCC, and FCC-Z) were designed on SolidWorks 2020-21. Unit cells of each lattice structure bearing the dimensions 2mm x 2mm x 2mm have been depicted in the figure 20. The initial phase of the design for each lattice structure was initiated by construction of struts. The struts were developed from cylindrical constructs designed with appropriate dimensional precision along X, Y and Z axes. Further, a linear pattern was employed on extruded cylinders to create a cubic structure of dimensions 8mm x 8mm x 8mm for the lattice. Two plates of thickness 1.5 mm, each added at the bottom and top of the specimen are to render support for the compression testing process.

A relation between the Porosity level (PL) and Cylinder Diameter (D) mathematically deduced for each lattice structure (Equations 2 to 5) [73] was employed to determine the diameter of the cylinder to obtain the right porosity levels.

$$PL_{BCC} = 61.686D^3 - 136.67D^2 + 0.2572\text{D} + 99.9 \quad \text{Equation 2}$$

$$PL_{BCC-Z} = 78.455D^3 - 160.1D^2 + 4.101\text{D} + 99.2 \quad \text{Equation 3}$$

$$PL_{FCC} = 48.737D^3 - 110.86D^2 - 0.0957\text{D} + 100.01 \quad \text{Equation 4}$$

$$PL_{FCC-Z} = 42.758D^3 - 86.889D^2 - 23.179\text{D} + 103.69 \quad \text{Equation 5}$$

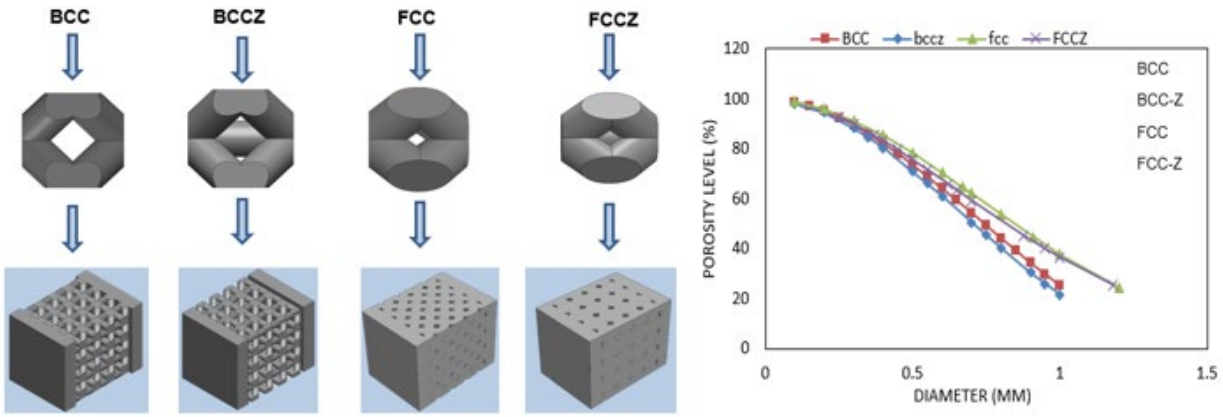

Figure 20: Graphical representation of relationship established between porosity level and strut diameter for each specimen.

Further, for Diamond, Gyroid, and Schwarz lattice structures, Mathematical equations (Equations 6 to 8) prescribed in a study carried out by Von Schnering, et. al. was considered to determine the nodal approximations [124].

$$\text{Diamond } F(x, y, z) = \cos(2\pi x).\sin(2\pi y) + \cos(2\pi y).\sin(2\pi z) + \cos(2\pi z).\sin(2\pi x) - K \quad \text{Equation 6}$$

$$\text{Gyroid } F(x, y, z) = \sin(2\pi x).\sin(2\pi y).\sin(2\pi z) + \sin(2\pi x).\cos(2\pi y).\cos(2\pi z) + \cos(2\pi x).\sin(2\pi y).\cos(2\pi z) + \cos(2\pi x).\cos(2\pi y).\sin(2\pi z) - K \quad \text{Equation 7}$$

$$\text{Schwarz } F(x, y, z) = \cos(2\pi x) + \cos(2\pi y) + \cos(2\pi z) - K \quad \text{Equation 8}$$

The ‘K’ in the equations is a constant used to effectively regulate the porosity levels.

K3Dsurf software was used to create the necessary coordinates for the surfaces of the porous parts and further the surfaces were created using Materialise Magics (Materialise 2020, Belgium) in a shell CAD format. The shell format of CAD files for each structure was then converted to their solid counterparts using the Solidworks.

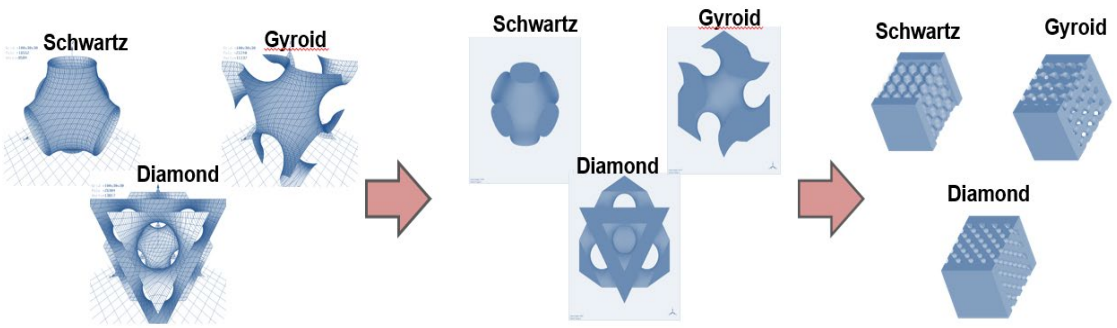

Figure 21: Designing of TPMS structures using K3Dsurf, Materialise Magics and Solidworks.

The equations (9 – 11) prescribed below were used to design the TPMS structures with a user-controlled approximation of porosity levels in the range of 10% - 90%.

$$PL_{Diamond} = 32.783K + 50.12 \quad \text{Equation 9}$$

$$PL_{Gyroid} = 42.284K + 50.12 \quad \text{Equation 10}$$

$$PL_{Schwartz} = 28.742K + 49.99 \quad \text{Equation 11}$$

The CAD files for the TPMS structures were created for 8mm x 8mm x 8mm maintaining a 45% porosity level along with two plates of 1.5mm thickness which are used on top and the bottom of the specimen during compression test.

3.3. Part Preparation for AM

The parts were modelled on a Computer aided design software, SolidWorks for the dimensions 8mm x 8mm x 8mm. The copies of the CAD files were also saved in their respective triangulated stereolithographic formats ensuring there were no losses in terms of design data. Further, the STL file is uploaded to Magics by Materialize (Materialize HQ, Berlin) to generate necessary support structures for the parts. Once the process of support generation is carried out, Process parameters are input on EOS Print 2 (EOS, Krailling, Germany). As a final step to the fabrication, the developed model is uploaded into the EOS M290 for fabrication.

3.4. Powder Preparation and Fabrication

The IN718 powder used in the fabrication is produced through the process of gas atomization and the composition is Ni (50-55 %), Cr (17 -21%), Nb (4.75-5.5%). With varied particle size with an average size of 40µm, the sieving process is carried out to eliminate particles larger than 75µm. Further, the powder is closely packed with minimum air gap to prevent defects during the fabrication process.

Figure 22: Retsch Sieve Machine.

IN718 alloy models were fabricated using an EOS M290 metal 3d printer with a build volume of 250 mm x 250 mm x 325 mm equipped with a 400-Watt Ytterbium fiber laser. Based on the layer thickness, the gap between the re-coater and the build plate. With the right alignment achieved, the initial powder layer is laid across the build plate at a specific layer thickness. Then, following a preset path and pattern defined by the uploaded file, high power laser melts the layer of IN718 powder. Following the solidification of the melted powder, successive layer is spread over the preceding layer. The laser path is dependent on the scan pattern and the raster pattern which was set and uploaded into the printer along with the other necessary parameters. For every successive layer of powder to be laid out the re-coater moves to its original position, along with re-coating the blade also removes excess powder to maintain uniformity of each layer. Initially, the supports are printed with a different parameter set to facilitate easier separation of the part from the supports and further each layer is solidified and successively fused to produce the target part.

Figure 23: EOS M290 Machine.

The components were fabricated at an energy density of 67 J/mm^2, the optimum setting for the fabrication. Further, Major parameters namely laser power (p) of 285W, layer thickness (t) of 40 µm, hatch spacing (h) of 110 µm, and scan speed (v) of 960 mm/sec was used throughout the entire fabrication process. Along with these process parameters, 'Stripes' scan strategy was adopted with an angle of 67^o changing between each layer.

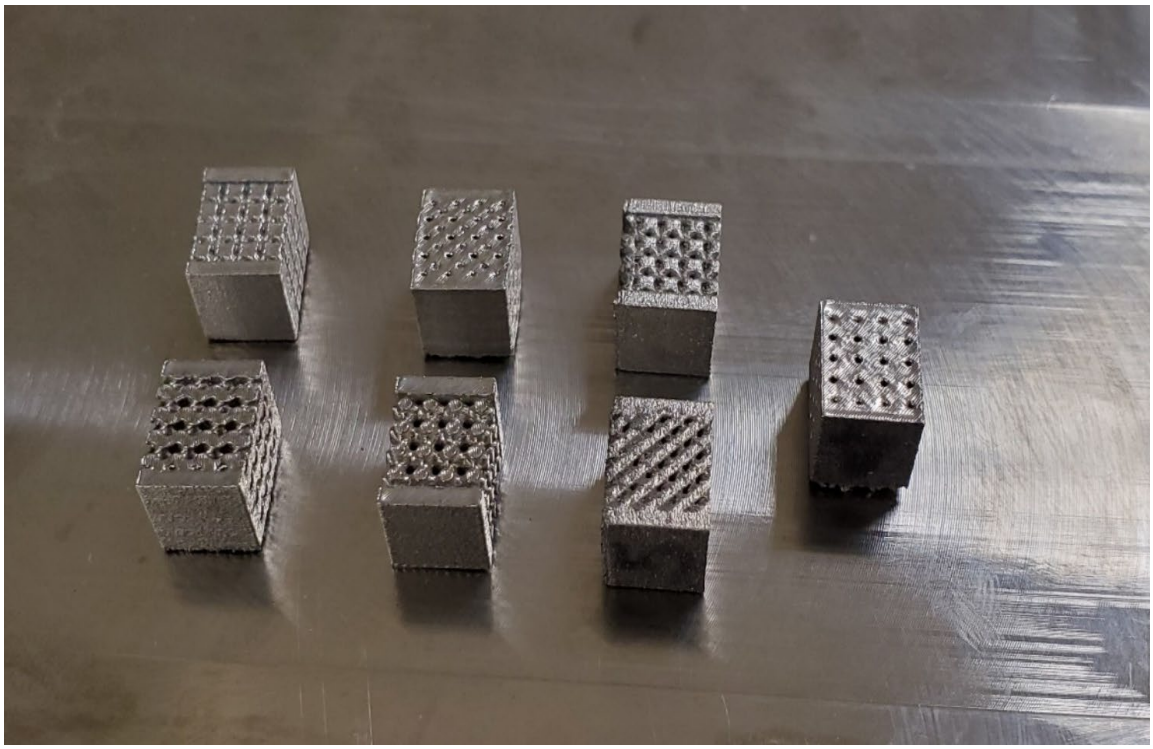

Figure 24: SLM fabricated samples on the stainless-steel build plate.

3.5. Experimental Procedures

Various attributes such as microstructure, metallurgical and mechanical properties of SLM fabricated IN718 samples was observed and recorded with several tests and experiments. The experimentation involved SEM analysis, compression tests along with DIC and finally Vickers hardness test.

3.5.1. Sample Preparation

Post fabrication, a band saw was used to separate the samples from the base plate. Further, supports were sheared off partially and the remnants were removed through the operation of grinding. Some of the samples necessary for XRD were prepared by cutting them perpendicular to the build direction with a thickness not greater than 2mm.

Figure 25: Allied Techcut 4.

Successively, the E-prep 4™ (Allied High-Tech Products, Inc., Rancho Dominguez, CA) was used for grinding and polishing operations to prepare the samples for SEM by facilitating a good surface finish. Furthermore, to prepare the samples for SEM, they were enclosed in epoxy resin and polished with Silicon Carbide (SiC) abrasives, with successive grit sizes ranging from 320 to 800 to decrease the opacity. Simultaneously the abrasion debris from the spin plate was carried out by flowing supply of water. A metallurgical microscope XJP- H100 (Amscope, Irvine, CA) was employed to inspect the uniformity on the surface of the samples.

Figure 26: Allied Prep - 4 Polishing Machine.

Further polishing was performed with the use of 1 μm diamond suspension on Dia Mat polishing cloth with Green Lube lubricant. The final involved the use of 0.04 μm colloidal silica suspension on a Chem-pol polishing cloth for finishing. Also, as a part of post processing the samples were cleaned in an ultrasonic bath and compressed air was used to clear the debris generated during handling. The samples were then etched with the use of Kroll's Reagent (1-3 mL HF, 2-6 mL HNO3, 100 mL water), prior to microstructural analysis.

3.5.2. Scanning Electron Microscope

SEM was carried out with the help of Hitachi S-3000N Variable Pressure SEM microscopy (Hitachi, Canada). The specimens were mounted on the holder with the use of double-sided carbon tape and the specimen holder's position was calibrated by adjusting the lock nut and the fastening screw. Next, the samples were moved into vacuum chamber and further placed into the SEM machine. Finally using SEM microscopy, the analysis process involved identification and measurements of profile and dimensions of the melt pools and grains, both in and away from the vicinity of the substrate. Further, precipitate composition for SLM IN718 specimens was evaluated for the same regions of the target areas as the SEM to learn the effect of scanning strategy on precipitate formation.

SEM was also performed on the mechanical test samples post rupture to learn the causes of failure in each sample.

Figure 27: Hitachi S-3000N Scanning Electron Microscope.

3.5.3. Hardness Measurements

The Vickers's hardness test for SLM IN718 samples were carried out on Metal-tester model 900-391D (LECO, St. Joseph's, MI, USA). The samples were sectioned into 4x4 grids on the as-fabricated surface on which the hardness indenter was utilized to estimate the hardness at each of the 16 test points. At each point, the indenter was perpendicularly loaded at 100g for 10 seconds. After indentation was performed on all the points, the indenter was moved, and the sample was placed under a microscopic lens with the crosshair aligned. With the alignment done at each point the hardness magnitude was evaluated. The same procedure was then consistently carried out on rest of the samples. Further the hardness was translated to 3D graphs, with build direction and the sample width as the axes against the hardness values.

Figure 28: LECO LM 300 AT Vickers hardness testing machine.

3.5.4. Mechanical Testing

Uniaxial compression test was performed using a Shimadzu EHF 100 Fatigue testing machine (Shimadzu Corporation, Kyoto Japan). The maximum compressive load of 83KN, and a strain rate of $10^{-4}sec^{-1}$ were applied. All samples were tested to the maximum load of 83KN, and the tests were evaluated with a graphical representation was employed in terms of load and displacement.

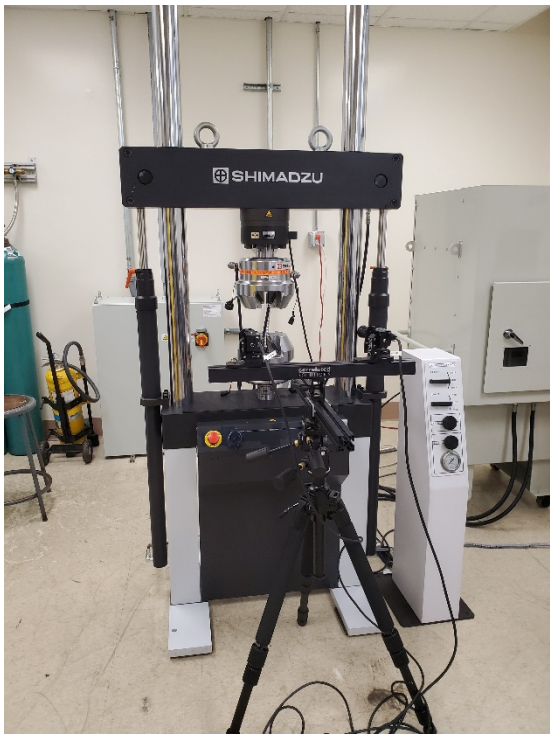

Figure 29: Shimadzu EHF100kN Fatigue Testing Machine.

Chapter 4. Results and Discussion

4.1. Fabricated Parts

The IN718 samples with various porous/lattice structures (BCC, BCC-Z, FCC, FCC-Z, Diamond, Gyroid, and Schwarz) were fabricated using SLM, the most common LPBF technique, on top of a Stainless-steel build plate. The porosity level of 45% and a stripe scan strategy was maintained during the fabrication of all the samples.

4.2. Mechanical Testing

4.2.1. Uniaxial Compression Test

The compression test was performed to a maximum of 83KN individually on all the specimens. BCC-Z and FCC-Z showed promising yield stresses of 946MPa and 965MPa, respectively, and FCC-Z having the highest value among all the porous types. Among the simple porous structures BCC, BCC-Z, FCC, and FCC-Z, a trend was observed between the Z-strut variants of both FCC and BCC where BCC-Z and FCC-Z displayed higher yields since the presence of Z-strut improved the resistance to yield also delaying the onset of compressive hardening. Comparing the TPMS structures, Diamond displayed the least magnitude for yield stress of 428MPa while Gyroid and Schwarz had the values of 523MPa and 526MPa, respectively. Also, considering the compressive displacements of all the specimens, Gyroid showed the maximum displacement of 4.836mm followed by Diamond with a value of 4.083mm while BCC exhibited the least displacement of 0.818mm followed by BCC-Z with a value of 0.813mm. The trend of BCC-Z and FCC-Z outperforming their non-modified counterparts can be seen in terms of compressive displacements as well. A detail tabular and graphical representations can be seen below containing various mechanical attributes for each porosity type.

Table 3: Yield stress, Failure stress and Failure strain for corresponding specimen type [125]

Specimen Type	Yield Stress (MPa)	Failure Stress (kN)	Failure Strain (mm/mm)
BCC	719	39.70	0.10
BCC-Z	946	50.60	0.22
FCC	558	61.20	0.28
FCC-Z	965	57.90	0.37
Gyroid	523	-	-
Schwatz	526	53.80	0.28
Diamond	428	-	-

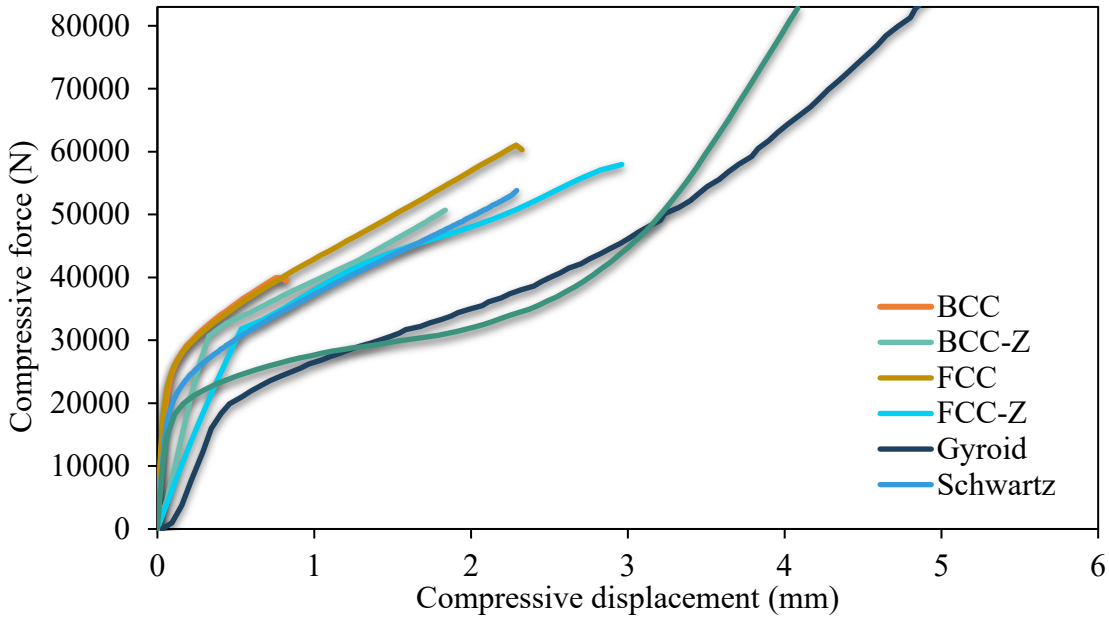

Figure 30: Graphical representation of compressive force and compressive displacements for each porosity type [125].

4.2.2. Hardness Analysis

The Vickers Hardness tests performed on each of the samples revealed Diamond bearing the highest hardness value of 421HV followed by BCC and BCC-Z with hardness values of 402HV and 378.5HV

respectively and the least value of hardness was observed in Gyroid with a magnitude of 337HV. A statistical comparison can be seen in the figure 28 below.

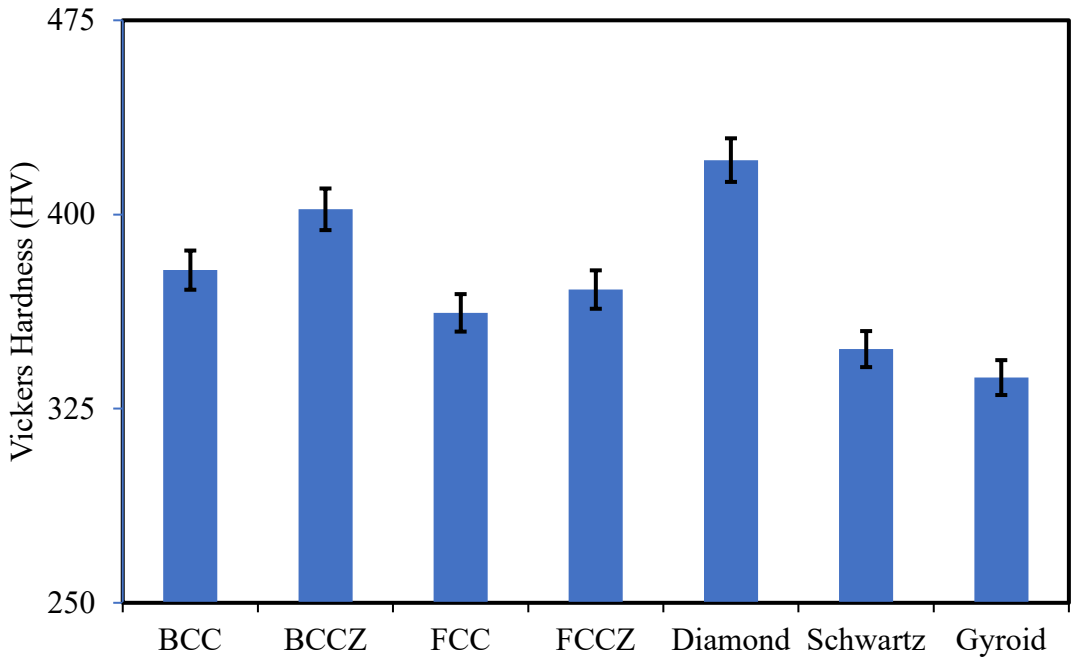

Figure 31: Vickers Hardness is displayed against each of the porosity type.

4.3. Microstructural Analysis

The main aspects involved in the microstructural analysis using SEM were to observe the melt pools, grain structures, defects and identify the changes in the shape of the unit cells of each of the specimens before and after uniaxial compressive tests.

4.3.1. Unit Cell Comparison

Considering the unit cells of the porosity type in the figure 27 below, it is evident that some of the specimens retained the shapes of their unit cells to a visible extent even after being subjected to compressive loads. Among all the samples, BCC, BCC-Z, FCC, FCC-Z and Schwarz porosity types can be seen retaining their unit cell shapes whereas Gyroid and Diamond displayed the maximum amount of deviation in the shape of their unit cells post compression. This observation can be associated to nature of the unit cell design. Unit cell designs in BCC, BCC-Z, FCC, FCC-Z and Schwarz have a similar trend of instantaneous

deviations in the profile of struts whereas the unit cells in Gyroid and Diamond show a smooth transition in the formation of each strut.

With unit cells in context a relationship between the unit cell structures and their corresponding compressive natures can be established. Considering the results from the compression, it can be observed that the Diamond and Gyroid due to the smooth transitive nature of their unit cells experience higher values of compressive displacements (4.083mm and 4.836mm respectively) while the rest of the types of porous structures lack in the same. With BCC and FCC structures showing lower values of compressive displacements, the Z-strut counterparts of each, the BCC-Z and FCC-Z structures display better results as the Z-struts are placed in the same direction of axial loading and the work hardening was delayed, hence prolonging the compression.

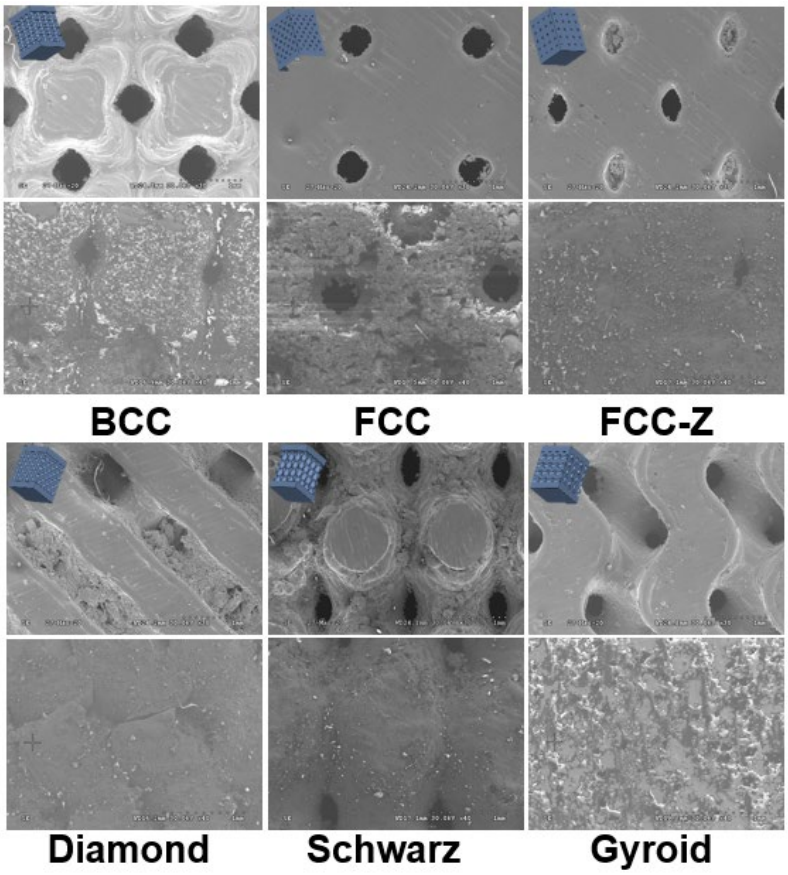

Figure 32: SEM images of unit cells of the specimen before (top) and after (bottom) compression.

4.3.2. Analysis for Meltpools and Defects

The meltpools and defects were observed at the same rate of magnification of SEM images. Some of the defects that were observed in the samples were partially/unmelted powder particles, cracks, pores, and precipitates. Though pores were only observed in negligible quantities, partially/ unmelted powder on the surface was observed in BCC, BCC-Z, FCC, FCC-Z, and Schwarz, which could be due to the instantaneous transition of profiles seen in the unit cells of these porosity types. Further, some cracks were found in BCC-Z and FCC-Z while considerably low amounts of precipitates could be observed in all the samples. These defects can have a direct impact on the mechanical properties as this would reduce the yield stress and reduce overall compressive displacement by leading to early failure of the parts. Some of the defects can be seen enclosed in the figure below.

Similarly, considering adjacent the meltpools of BCC, BCC-Z, FCC, FCC-Z, and Schwarz had irregularities in the width and depths which could again be attributed to the nature of their unit cells. The adjacent meltpools of Gyroid and Diamond were observed to have uniformity in terms of width and depth, and this can also be attributed to their respective natures of unit cells. Varying size of meltpools tend to reduce the yield stress whereas uniformity in the meltpools can lead to give the part a consistent yield results under compression. The meltpools of each sample can be visualized below in the figure.

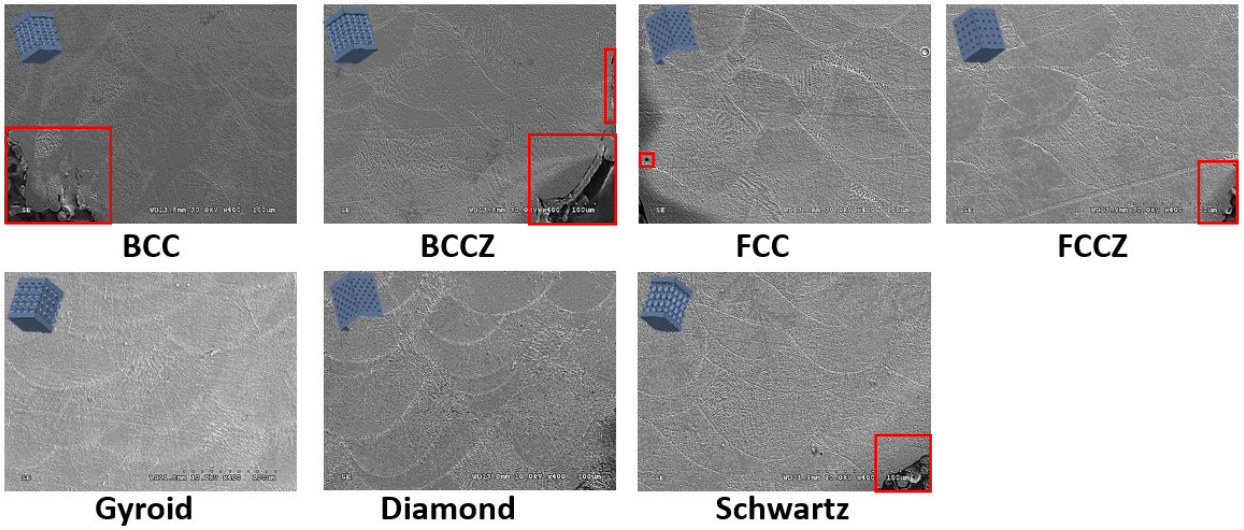

Figure 33: Meltpools and defects observed in each sample. (The strut surfaces of each of the porous structures were visualized for SEM).

4.3.3. Grain Structure Analysis

The grain structure, isotropic distribution of grains has direct impact on the mechanical properties. Anisotropy and varying grain shapes and structure observed in the SEM images of each of the samples can significantly reduce the compressive strength hence reducing yield stress and compressive displacement. A similar trend as seen earlier can be recognized even terms of grain structures of each porosity type and the same can again be attributed to the nature of the unit cell. BCC, BCC-Z, FCC, FCC-Z and Schwarz displayed irregularities in terms of the grain structure, grain shapes, and grain sizes at various regions. In the case of Gyroid and Diamond, Gyroid displaying a notable and maximum amount of isotropy along with fine grain structures whereas Diamond also showed a significant number of columnar grains with considerable amounts of grain isotropy but stood second in comparison with Gyroid. The figure 31 below provides a visual of the grain structure through SEM images.

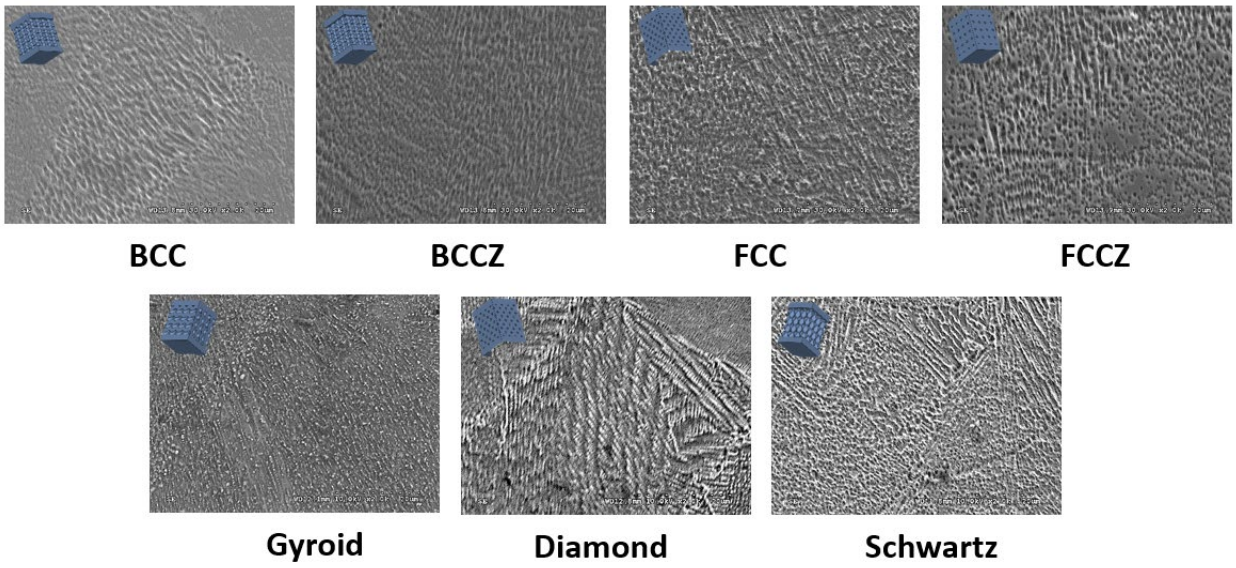

Figure 34: SEM images showing the grain structures.

Chapter 5. Conclusions and Future Works

5.1. Conclusions

Considering the results from the mechanical tests and microstructural analysis, the following conclusions were made:

(i) The compression results showed a particular trend that was seen in the BCC, FCC and their Z-strut counterparts BCC-Z and FCC-Z. Noteworthy, BCC-Z and FCC-Z outperformed their simple/non modified forms in terms of compressive displacements and mechanical strengths which can be linked to the presence of Z-struts experiencing majority and simultaneously resisting the compressive loads. Among all the porous types, Gyroid displayed promising results by exhibiting the highest value of compressive displacement but lacked yield stress. Moreover, FCC-Z showed the best result in terms of yield stress followed by BCC-Z.

(ii) The microstructural results revealed the dependence of mechanical properties on the nature of unit cells of each porosity type. Upon comparing the SEM images of the unit cells prior and post compression test, the smooth transition in the design of structures such as Gyroid and Diamond was advantageous in prolonging the hardening phase hence leading to higher compressive displacements. On the contrary, simple porous structures such as BCC, BCC-Z, FCC, FCC-Z and Schwarz having a similar instantaneous change in the design of their struts along their unit cells attained early failure.

(iii) Further, examining the grain structures which can again be linked with the nature of the unit cells, Gyroid can be seen having a fine and uniform grain structure and diamond with similar uniformity and isotropy of columnar grains. However, the other porous types displayed irregularities and anisotropic grain structures. Considering the impact grain structures have on the mechanical properties, it can be concluded that anisotropy and varying grain sizes and structures can lead to early failures and reduced compressive displacements.

(iv) Defects also a play a significant role in contributing to the mechanical stability of a part. With that in context, several defects such as pores, cracks, precipitates, and unmelted/partially melted powder was

observed more in structures such as BCC, BCC-Z, FCC, FCC-Z, and Schwarz when compared to Diamond and Gyroid. Again, the proportions of defects can be linked to the nature of transition of the strut design in each unit cell.

(v) Finally, Diamond showed the highest hardness, and a superior trend was observed in BCC-Z and FCC-Z compared to their simpler counterparts while Gyroid and Schwarz exhibiting low hardness values.

Considering the results, a bridging conclusion can be drawn by establishing a strong relationship for porosity type with both mechanical and microstructural properties with a critical emphasis on the nature of the unit cell design.

5.2. Future Work

This study focused on establishing a relationship between the porosity type, mechanical properties, and their corresponding microstructural attributes. While the investigation addressed the inquiries of the above-mentioned aspects, it also created scope and opened new opportunities into exploring the following:

- The study remained short on providing the necessary reasoning for the hardness values of each porosity type.
- A future work involving tensile and fatigue tests would further strengthen the understanding of the effect of microstructural and mechanical properties on the porosity types.

References

1. Chang, C., et al., Microstructure and mechanical deformation behavior of selective laser melted Ti6Al4V ELI alloy porous structures. Materials Letters, 2020. 277.
2. Reed, R.C., The Superalloys Fundamentals and Applications. 2008: Cambridge university press.
3. Zheng, L., et al., Mechanism of Intermediate Temperature Embrittlement of Ni and Ni-based Superalloys. Critical Reviews in Solid State and Materials Sciences, 2012. 37(3): p. 181-214.
4. Paulonis, D.F.a.J.J.S., Alloy 718 at Pratt & Whitney–Historical perspective and future challenges. Superalloys. 2001.
5. Newton, T.R., Investigation of the effect of process parameters on the formation and characteristics of recast layer in wire-EDM of Inconel 718, in Materials Science and Engineering. 2009, Georgia Institute of Technology.
6. Iturbe, A., et al., Mechanical characterization and modelling of Inconel 718 material behavior for machining process assessment. Materials Science and Engineering: A, 2017. 682: p. 441-453.
7. Blaine Geddes, H.L., Xiao Huang, Superalloys: alloying and performance. Asm International, 2010.
8. L. Garimella, P.K.L., and D.L. Klarstrom Fatigue behavior in nickel-based superalloys: A literature review. Jom, 1997.
9. Uginet*, B.P.a.J.F., FATIGUE AND CREEP PROPERTIES IN RELATION WITH ALLOY 718 MICROSTRUCTURE. Superalloys. 1994.
10. Ardila, L.C., et al., Effect of IN718 Recycled Powder Reuse on Properties of Parts Manufactured by Means of Selective Laser Melting. Physics Procedia, 2014. 56: p. 99-107.
11. Brooks, J.a.P.B., Metallurgical stability of Inconel alloy 718. Superalloys. 1988.
12. Bharath Bhushan, R., Correlation and effect of process parameters on the properties of inconel 718 parts fabricated by selective laser melting using response surface method, in Mechanical Engineering. 2020, The University of Texas at Arlington: Arlington, TX.

13. Azadian, S., L.-Y. Wei, and R. Warren, Delta phase precipitation in Inconel 718. Materials characterization. 2004.

14. G.A. KNOROVSKY, M.J.C., T.J. HEADLEY, A.D. ROMIG, Jr., and W. E HAMMETTER, INCONEL 718 A Solidification Diagram. Metallurgical Transactions, 1989. 20A(2149–2158).

15. David J. Newell, M., USAF, SOLUTION ANNEAL HEAT TREATMENT TO ENHANCE MECHANICAL PERFORMANCE OF ADDITIVELY MANUFACTURED IN718, in Graduate School of Engineering and Management. 2020: Wright-Patterson Air Force Base, Ohio.

16. Scallan, P., Material evaluation and process selection. Process Planning. 2003

17. Donachie, M.J.a.S.J.D., Superalloys: a technical guide. ASM international, 2002.

18. Jing Li, Z.Z., Peikang Bai, Hongqiao Qu, Bin Liu, Liang Li, Liyun Wu, Renguo Guan, Hu Liu, Zhanhu Guo, Microstructural evolution and mechanical properties of IN718 alloy fabricated by selective laser melting following different heat treatments,

. Journal of Alloys and Compounds, 2019. Volume 772.

19. Carlson, R.G.a.J.F.R., MICROSTRUCTURAL CHARACTERIZATION OF CAST 718. International Symposium on Superalloys, 1989.

20. Borg, C.A., R.W. Hatala, and J.J. Schirra, Characterization of vacuum die cast Inconel 718 and

derivatives (PWA 1472/PWA 1473). Superalloys 718, 625, 706 and Various Derivatives. 2001.

21. Rao, G.A., M. Srinivas, and D.S. Sarma,, Effect of standard heat treatment on the microstructure and mechanical properties

of hot isostatically pressed superalloy Inconel 718. Materials Science and Engineering: A, 2003.

22. Moghaddam, N., et al., Stiffness Tuning of Niti Implants Through Aging. V001T02A014-V001T02A014, 2016.

23. Rao, G.A., M. Srinivas, and D.S. Sarma, Influence of modified processing on structure and

properties of hot isostatically pressed superalloy Inconel 718. Materials Science and Engineering, 2006.

24. Rao, G.A., M. Srinivas, and D.S. Sarma, Effect of oxygen content of powder on microstructure and mechanical properties of hot isostatically pressed superalloy Inconel 718. Materials Science and Engineering, 2006.

25. https://www.thomasnet.com/articles/custom-manufacturing-fabricating/casting-materials/.

26. http://www.elite-alloys.com/wrought-products.

27. Kiriti, M., et al. Study on the influence of post-processing parameters over microstructure and metallurgical properties of NiTi alloy. in Proc.SPIE. 2020.

28. https://www.mpif.org/IntrotoPM/Processes/IsostaticPressing.aspx.

29. Ibrahim, H., et al., In vitro corrosion assessment of additively manufactured porous NiTi structures for bone fixation applications. Metals, 2018. 8(3): p. 164.

30. Jahadakbar, A., et al., Finite element simulation and additive manufacturing of stiffness-matched niti fixation hardware for mandibular reconstruction surgery. Bioengineering, 2016. 3(4): p. 36.

31. Dehghanghadikolaei, A., et al., Improving corrosion resistance of additively manufactured nickel–titanium biomedical devices by micro-arc oxidation process. Journal of materials science, 2019. 54(9): p. 7333-7355.

32. Moghaddam, N.S., et al., Achieving superelasticity in additively manufactured NiTi in compression without post-process heat treatment. Scientific reports, 2019. 9(1): p. 1-11.

33. Attaran, M., The advantages of additive manufacturing over traditional

manufacturing. Business Horizons. Vol. 60(5). 2017.

34. Farhang, B., et al., Study on variations of microstructure and metallurgical properties in various heat-affected zones of SLM fabricated Nickel–Titanium alloy. Materials Science and Engineering: A, 2020. 774: p. 138919.

35. Elahinia, M., et al., Fabrication of NiTi through additive manufacturing: A review. Progress in Materials Science, 2016. 83: p. 630-663.

36. Andani, M.T., et al., Metals for bone implants. Part 1. Powder metallurgy and implant rendering. Acta biomaterialia, 2014. 10(10): p. 4058-4070.

37. Ahmadi, A., et al., Effect of manufacturing parameters on mechanical properties of 316L stainless steel parts fabricated by selective laser melting: A computational framework. Materials & Design, 2016. 112: p. 328-338.

38. Esfahani, S.N., et al., Independent tuning of stiffness and toughness of additively manufactured titanium-polymer composites: Simulation, fabrication, and experimental studies. Journal of Materials Processing Technology, 2016. 238: p. 22-29.

39. Saedi, S., et al., Shape memory response of porous NiTi shape memory alloys fabricated by selective laser melting. Journal of Materials Science: Materials in Medicine, 2018. 29(4): p. 1-12.

40. Amerinatanzi, A., et al., Application of the superelastic NiTi spring in ankle foot orthosis (AFO) to create normal ankle joint behavior. Bioengineering, 2017. 4(4): p. 95.

41. Saedi, S., et al., On the effects of selective laser melting process parameters on microstructure and thermomechanical response of Ni-rich NiTi. Acta Materialia, 2018. 144: p. 552-560.

42. Saedi, S., et al., Texture, aging, and superelasticity of selective laser melting fabricated Ni-rich NiTi alloys. Materials Science and Engineering: A, 2017. 686: p. 1-10.

43. Elahinia, M., et al., Additive manufacturing of NiTiHf high temperature shape memory alloy. Scripta Materialia, 2018. 145: p. 90-94.

44. Ma, C., et al., Improving surface finish and wear resistance of additive manufactured nickel-titanium by ultrasonic nano-crystal surface modification. Journal of Materials Processing Technology, 2017. 249: p. 433-440.

45. Moghaddam, N.S., et al., Anisotropic tensile and actuation properties of NiTi fabricated with selective laser melting. Materials Science and Engineering: A, 2018. 724: p. 220-230.

46. Moghaddam, N.S., et al., Metals for bone implants: Safety, design, and efficacy. Biomanufacturing Reviews, 2016. 1(1): p. 1-16.

47. Moghaddam, N.S., et al., Three dimensional printing of stiffness-tuned, nitinol skeletal fixation hardware with an example of mandibular segmental defect repair. Procedia Cirp, 2016. 49: p. 45-50.

48. Deckard, C.a.J.B., Selective Laser Sintering. Birth of an Industry. 2012.

49. Deckard, C.R., Method and apparatus for producing parts by selective sintering. 1986, USA.

50. Shayesteh Moghaddam, N., et al., Fixation release and the bone bandaid: A new bone fixation device paradigm. Bioengineering, 2017. 4(1): p. 5.

51. Shayesteh Moghaddam, N., Toward patient specific long lasting metallic implants for mandibular segmental defects. 2015, University of Toledo.

52. Saghaian, S., et al., Mechanical and shape memory properties of triply periodic minimal surface (TPMS) NiTi structures fabricated by selective laser melting. Biol. Eng. Med, 2018. 3: p. 1-7.

53. Ashrafi, M.J., et al., Shape memory response of cellular lattice structures: Unit cell finite element prediction. Mechanics of Materials, 2018. 125: p. 26-34.

54. https://www.ge.com/additive/additive-manufacturing/industries/aviation-aerospace.

55. Harbaugh, J. Space Station 3-D Printer Builds Ratchet Wrench To Complete First Phase Of Operations. 2014; Available from: https://www.nasa.gov/mission_pages/station/research/news/3Dratchet_wrench.

56. V, W.J.S., ADDITIVE MANUFACTURING OF INCONEL 718 USING ELECTRON BEAM MELTING: PROCESSING, POST-PROCESSING, & MECHANICAL PROPERTIES. 2015, Texas A&M University.

57. Thomas, D., The Development of Design Rules for Selective Laser Melting in The National Centre for Product Design & Development Research 2009 University of Wales Institute, Cardiff.

58. Baufeld, B., E. Brandl, and O.V.d. Biest, Wire based additive layer manufacturing: Comparison of microstructure and mechanical properties of Ti–6Al–4V components fabricated by laser-beam deposition and shaped metal deposition. Journal of Materials Processing Technology, 2011.

59. Andersen, P.J.a.S.K.H., Articles of manufacture and methods for manufacturing laminate structures including inorganically filled sheets. 1998.

60. Gibson, I., D. Rosen, and B. Stucker, Additive Manufacturing Technologies. Vol. 2 ed. 2015.

61. Sourabh, T., et al. The effect of support structure geometry on surface topography of selectively laser melted parts. in Proc.SPIE. 2020.

62. Ganesh-Ram, A., et al., Study on the microstructural and hardness variations of unsupported overhangs fabricated using selective laser melting, in Behavior and Mechanics of Multifunctional Materials XV. 2021.

63. https://noizear.com/crystallon-lattice-structures-in-rhino-and-grasshopper/.

64. Ravichander, B.B., A. Amerinatanzi, and N. Shayesteh Moghaddam, Study on the Effect of Powder-Bed Fusion Process Parameters on the Quality of as-Built IN718 Parts Using Response Surface Methodology. Metals, 2020. 10(9).

65. Trosch, T., et al., Microstructure and mechanical properties of selective laser melted Inconel 718 compared to forging and casting. Materials Letters, 2016. 164: p. 428-431.

66. Gu, D., et al., Densification behavior, microstructure evolution, and wear performance of selective laser melting processed commercially pure titanium. Acta Materialia, 2012. 60(9): p. 3849-3860.

67. Pröbstle, M.N., S.; Hopfenmüller, J.; Freund, L.; Niendorf, T.; Schwarze, D.; Göken, M., Superior creep strength of a nickel-based superalloy produced by selective laser melting. Materials Science and Engineering: A,, 2016. Volume 674: p. 299-307.

68. Bharath Bhushan, R., et al. Analysis of the deviation in properties of selective laser melted samples fabricated by varying process parameters. in Proc.SPIE. 2020.

69. Yan, C., et al, Evaluations of cellular lattice structures manufactured using selective laser melting.

. International Journal of Machine Tools and Manufacture, 2012.

70. Haase, C., et al., Exploiting process-related advantages of selective laser melting for the production of high-manganese steel. Materials 2017: p. p. 56.

71. Galy, C., et al., Main defects observed in aluminum alloy parts produced by SLM: From causes to consequences. Additive Manufacturing, 2018. 22: p. 165-175.

72. Gong, H., et al., Influence of defects on mechanical properties of Ti–6Al–4V components produced by selective laser melting and electron beam melting. Materials & Design, 2015. 86: p. 545-554.

73. Srivathsan, S., et al., Investigation of the strength of different porous lattice structures manufactured using selective laser melting, in Behavior and Mechanics of Multifunctional Materials IX. 2020.

74. Srihari, S., et al. Investigation of the strength of different porous lattice structures manufactured using selective laser melting. in Proc.SPIE. 2020.

75. Shellabear, M.a.O.N., DMLS-Development history and state of the art. Laser Assisted Netshape engineering proceedings of the 4th LANE, 2004.

76. Kruth, J.-P., et al., Binding mechanisms in selective laser sintering and selective laser melting. Rapid prototyping journal, 2005.

77. Xiao, B.a.Y.Z., Numerical simulation of direct metal laser sintering of single-component powder on top of sintered layers. Journal of manufacturing science and engineering, 2008.

78. Nyrhilae, M.S.a.O., DMLS - DEVELOPMENT HISTORY AND STATE OF THE ART, in LANE 2004 conference. 2004: Erlangen, Germany.

79. Aytimur, A.K., Serhat & Uslu, Ibrahim, Calcia Stabilized Ceria Doped Zirconia Nanocrystalline Ceramic. Journal of Inorganic and Organometallic Polymers and Materials, 2014. 24(10).

80. R. Singh, S.S., M.S.J. Hashmi, Implant Materials and Their Processing Technologies. Reference Module in Materials Science and Materials Engineering, Elsevier, 2016.

81. Shi, J.Z., Liya & Li, Lan & Li, Zongan & Yang, Jiquan & Wang, Xingsong, A TPMS-based method for modeling porous scaffolds for bionic bone tissue engineering. Scientific Reports, 2018. 8(1038/s41598-018-25750-9).

82. Yan, C., et al., Evaluations of cellular lattice structures manufactured using selective laser melting. International Journal of Machine Tools and Manufacture, 2012. 62: p. 32-38.

83. SRIVATHSAN, S., MODELING, FABRICATION, AND CHARACTERIZATION OF POROUS INCONEL 718 STRUCTURES USING SELECTIVE LASER MELTING PROCESS, in Mechanical and Aerospace Engineering. 2020, The University of Texas at Arlington.

84. Bharath Bhushan Ravichander, B.F., Nahid Swails, Amirhesam Amerinatanzi, Narges Shayesteh Moghaddam, Analysis of the deviation in properties of selective laser melted samples fabricated by varying process parameters. Proc. SPIE 11377, Behavior and Mechanics of Multifunctional Materials IX, 2020.

85. Bharath Bhushan, R., et al. A framework for the optimization of powder-bed fusion process. in Proc.SPIE. 2021.

86. Bharath Bhushan, R., et al. Development of ANN model for surface roughness prediction of parts produced by varying fabrication parameters. in Proc.SPIE. 2021.

87. Nakajima, H., Fabrication, properties and application of porous metals with directional pores. Progress in Materials Science, 2007. 52(7).

88. Williams, C.B., J.K. Cochran, and D.W. Rosen, Additive manufacturing of metallic cellular materials via three-dimensional printing. The International Journal of Advanced Manufacturing Technology, 2011.

89. Du, Y., et al., Laser additive manufacturing of bio-inspired lattice structure: Forming quality, microstructure and energy absorption behavior. Materials Science and Engineering: A, 2020. 773.

90. Ashby, M.F.a.L.J.G., Cellular solids: structure and properties. 1997, Cambridge, UK: Press Syndicate of the University of Cambridge.

91. Mazur, M., et al, Deformation and failure behaviour of Ti-6Al-4V lattice structures manufactured by selective laser melting (SLM). The International Journal of Advanced Manufacturing Technology, 2016(84(5-8)): p. 1391-1411.

92. Ushijima, K., et al., An investigation into the compressive properties of stainless steel micro-lattice structures. Journal of Sandwich Structures & Materials, 2011. 13(3): p. p. 303-329.

93. Ushijima, K., W. Cantwell, and D. Chen, Prediction of the mechanical properties of micro-lattice structures subjected to multi-axial loading. International Journal of Mechanical Sciences, 2013. 68: p. 47-55.

94. Gümrük, R., R. Mines, and S. Karadeniz, Static mechanical behaviours of stainless steel micro lattice structures under different loading conditions. Materials Science and Engineering, 2013. 586: p. 392-406.

95. Tancogne-Dejean, T.a.D.M., Stiffness and specific energy absorption of additively manufactured metallic BCC metamaterials composed of tapered beams. International Journal of Mechanical Sciences, 2018. 141: p. 101-116.

96. Leary, M., et al, Selective laser melting (SLM) of AlSi12Mg lattice structures. Materials & Design, 2016. 98: p. 344-357.

97. Mazur, M., et al., Mechanical properties of Ti6Al4V and AlSi12Mg lattice structures manufactured by Selective Laser Melting (SLM), in Laser Additive Manufacturing. 2017. p. 119-161.

98. Sienkiewicz, J., et al., Investigations on the Mechanical Response of Gradient Lattice Structures Manufactured via SLM. Metals, 2020. 10(2).

99. Deng, Y.a.M.M., Three-dimensional periodic cubic membrane structure in the mitochondria of amoebaeChaos carolinensis. Protoplasma, 1998. 203(1-2): p. 16-25.

100. Jiang, S., A. Göpfert, and V. Abetz, Novel morphologies of block copolymer blends via hydrogen bonding. . Macromolecules, 2003. 36(16): p. 6171-6177.

101. Cartwright, J.H.a.A.L.M., Beyond crystals: the dialectic of materials and information. The Royal Society Publishing, 2012.

102. Schwarz, H.A., Gesammelte mathematische abhandlungen. American Mathematical Soc., 1972. Vol. 260.

103. Schoen, A.H., Infinite periodic minimal surfaces without self-intersections. National Aeronautics and Space Administration, 1970.

104. Karcher, H., The triply periodic minimal surfaces of Alan Schoen and their constant mean curvature companions. Manuscripta mathematica, 1989. 64(3): p. 291-357.

105. Zhang, L., et al., Energy absorption characteristics of metallic triply periodic minimal surface sheet structures under compressive loading. Additive Manufacturing, 2018. 23: p. 505-515.

106. Zhao, M., et al., Improved Mechanical Properties and Energy Absorption of BCC Lattice Structures with Triply Periodic Minimal Surfaces Fabricated by SLM. Materials (Basel), 2018. 11(12).

107. Vignesh, R.K.R., et al. Determination of residual stress for Inconel 718 samples fabricated through different scanning strategies in selective laser melting. in Proc.SPIE. 2020.

108. Sing, S.L., F.E. Wiria, and W.Y. Yeong, Selective laser melting of lattice structures: A statistical approach to manufacturability and mechanical behavior. Robotics and Computer-Integrated Manufacturing,, 2018. 49:: p. 170-180.

109. Xiao, Z., et al, Evaluation of topology-optimized lattice structures manufactured via selective laser melting. Materials & Design, 2018. 143: p. 27-37.

110. Wauthle, R., et al., Effects of build orientation and heat treatment on the microstructure and mechanical properties of selective laser melted Ti6Al4V lattice structures. Additive Manufacturing, 2015. 5: p. 77-84.

111. Maskery, I., et al, A mechanical property evaluation of graded density Al-Si10-Mg lattice structures manufactured by selective laser melting. Materials Science and Engineering: A, 2016. 670: p. 1755-1769.

112. Gong, H., et al., Influence of defects on mechanical properties of Ti–6Al–4 V components produced by selective laser melting and electron beam melting. Materials & Design, 2015. 86: p. 545-554.

113. Maconachie, T., et al., SLM lattice structures: Properties, performance, applications and challenges. Materials & Design, 2019: p. 108-137.

114. Bharath Bhushan, R., A. Amirhesam, and M. Narges Shayesteh. Toward mitigating microcracks using nanopowders in laser powder bed fusion. in Proc.SPIE. 2021.

115. Manjunath, H., et al. Spatial microstructural analysis for selective laser melted components. in Proc.SPIE. 2021.

116. Choy, S.Y., et al., Compressive properties of Ti-6Al-4V lattice structures fabricated by selective laser melting: Design, orientation and density. Additive Manufacturing, 2017: p. 213-224.

117. Santorinaios, M., et al., Crush behaviour of open cellular lattice structures manufactured using selective laser melting. WIT transactions on the built environment, 2006. 85.

118. McKown, S., et al., The quasi-static and blast loading response of lattice structures. International Journal of Impact Engineering

2008. 35(8): p. 795-810.

119. Pattanayak, D.K., et al., Bioactive Ti metal analogous to human cancellous bone: fabrication by selective laser melting and chemical treatments. Acta Biomaterialia, 2011. 7(3): p. 1398-1406.

120. Qiu, C., et al., Influence of processing conditions on strut structure and compressive properties of cellular lattice structures fabricated by selective laser melting. Materials Science and Engineering, 2015. 628: p. 188-197.

121. Koehnen, P., et al., Mechanical properties and deformation behavior of additively manufactured lattice structures of stainless steel. Materials & Design, 2018. 145: p. 205-217.

122. Shahir Mohd Yusuf, S.C., Nong Gao Review: The Impact of Metal Additive Manufacturing on the Aerospace Industry. Metals, 2019. 9(12)(1286).

123. Zadi-Maad, A., Additive manufacturing for steels: a review, in MINEPROCET 2017. 2017.

124. Von Schnering, H.a.R.N., Nodal surfaces of Fourier series: fundamental invariants of structured matter. Zeitschrift für Physik B Condensed Matter, 1991. 83(3): p. 407-412.

125. Srivathsan, S., et al. Investigation of the strength of different porous lattice structures manufactured using selective laser melting. in Behavior and Mechanics of Multifunctional Materials IX. 2020. International Society for Optics and Photonics.